EUROPEAN RESPIRATORY *journal*

FLAGSHIP SCIENTIFIC JOURNAL OF ERS

Early View

Original article

Targeting TMEM16A to reverse vasoconstriction and remodelling in idiopathic PAH

Rita Papp, Chandran Nagaraj, Diana Zabini, Bence M. Nagy, Miklós Lengyel, Davor Skofic Maurer, Neha Sharma, Bakytbek Egemnazarov, Gabor Kovacs, Grazyna Kwapiszewska, Leigh M. Marsh, Andelko Hrzenjak, Gerald Höfler, Miroslava Didiasova, Malgorzata Wygrecka, Laura Sievers, Peter Szucs, Péter Enyedi, Bahil Ghanim, Walter Klepetko, Horst Olschewski, Andrea Olschewski

Please cite this article as: Papp R, Nagaraj C, Zabini D, *et al*. Targeting TMEM16A to reverse vasoconstriction and remodelling in idiopathic PAH. *Eur Respir J* 2019; in press (https://doi.org/10.1183/13993003.00965-2018).

Targeting TMEM16A to reverse vasoconstriction and remodeling in idiopathic PAH

Rita Papp[1*], Chandran Nagaraj[1*], Diana Zabini[1,2], Bence M. Nagy[1], Miklós Lengyel[3], Davor Skofic Maurer[2], Neha Sharma[1],Bakytbek Egemnazarov[1], Gabor Kovacs[1,4], Grazyna Kwapiszewska[1], Leigh M. Marsh[1], Andelko Hrzenjak[1,4], Gerald Höfler[5], Miroslava Didiasova[6], Malgorzata Wygrecka[6], Laura Sievers[7], Peter Szucs[8], Péter Enyedi[3], Bahil Ghanim[9], Walter Klepetko[9], Horst Olschewski[4], Andrea Olschewski[1,2#]

[1]Ludwig Boltzmann Institute for Lung Vascular Research, Graz, Austria

[2]Department of Physiology, Medical University of Graz, Graz, Austria

[3]Department of Physiology, Faculty of Medicine, Semmelweis University, Budapest, Hungary

[4]Division of Pulmonology, Department of Internal Medicine, Medical University of Graz, Graz, Austria

[5]Department of Pathology, Medical University of Graz, Graz, Austria

[6]Department of Biochemistry, Universities of Giessen and Marburg Lung Center, Giessen, Germany

[7]Medical Clinic D, University Clinic of Münster, Münster, Germany

[8]Department of Anatomy, Histology and Embriology, University of Debrecen, Debrecen, Hungary

[9]Division of Thoracic Surgery, Department of Surgery, Medical University of Vienna, Vienna, Austria

*contributed equally

#Corresponding Author: Prof. Andrea Olschewski

Stiftingtalstrasse 24, Graz, A-8010, Austria

Telephone: +43 (0)316 385-72057

Fax: +43 (0)316 385-72058

Email: Andrea.Olschewski@lvr.lbg.ac.at

Author contributions: R.P., C.N., D.Z., B.M.N., D.S.M., N.S., M.L., P.E., G.Kovacs, H.O. and A.O. designed experiments, and acquired, analyzed and interpreted data. B.E. and M.D.

acquired and analyzed data. G. Kwapiszewska, L.M.M., A.H., and P.S. contributed to the study design with ideas and/or technical advice. G.H., M.W., L.S., B.G and W.K. provided either infrastructure or experimental material. R.P., H.O., D.Z. and A.O. prepared the manuscript. C.N., B.M.N., G. Kovacs, G. Kwapiszewska, L.M.M., A.H., M.D., M.W., and L.S. gave valuable advice on manuscript preparation.

Grant support: AO is supported by OeNB(16682); M.L. was supported by the New National Excellence Program of the Ministry of Human Capacities (ÚNKP-18-3-III-SE-43).

Subject code: 17.06, 3.15; 17.04; 17.10; 3.10

At a Glance Commentary:

Scientific Knowledge on the Subject:

Though chloride channels have long been known to be present in pulmonary arterial smooth muscle cells, little attention has been paid to anion channels and transporters in pulmonary arterial hypertension (PAH).

What This Study Adds to the Field:

Our *in vitro* and *in vivo* experiments suggest that the Ca^{2+}-sensitive Cl^- channel TMEM16A plays a central role in the pathologic mechanisms underlying depolarization, vasoconstriction and proliferation of PASMC, contributing to the increased pulmonary vascular resistance in PAH. TMEM16A provides an important novel target for PAH therapy.

"This article has an online data supplement, which is accessible from this issue's table of contents online at www.atsjournals.org"

Abstract

Rationale:

Our systematic analysis of anion channels and transporters in idiopathic pulmonary arterial hypertension (IPAH) showed marked upregulation of the Cl^- channel TMEM16A gene.

Objective:

We hypothesized that TMEM16A overexpression might represent a novel vicious circle in the molecular pathways causing PAH.

Methods and results:

We investigated healthy donor lungs (n=40) and recipient lungs with IPAH (n=38) for the expression of anion channel and transporter genes in small pulmonary arteries and pulmonary arterial smooth muscle cells (PASMC). In IPAH, TMEM16A was strongly upregulated and patch-clamp recordings confirmed an increased Cl^- current in PASMC (n=9-10). These cells were depolarized and could be repolarized by TMEM16A inhibitors or knock-down experiments (n=6-10). Inhibition/knock-down of TMEM16A reduced proliferation of IPAH-PASMC (n=6). Conversely, overexpression of TMEM16A in healthy donor PASMC produced an IPAH-like phenotype. Chronic application of benzbromarone in two independent animal models significantly decreased right ventricular pressure and reversed remodeling of established PH.

Conclusion:

Our findings suggest that increased TMEM16A expression and activity comprise an important pathologic mechanism underlying vasoconstriction and remodeling of pulmonary arteries in PAH. Inhibition of TMEM16A represents a novel therapeutic approach to achieve reverse remodeling in PAH.

Introduction

Idiopathic pulmonary arterial hypertension (IPAH) is a rare disease characterized clinically by the constriction of precapillary pulmonary arteries and associated with irreversible remodeling. The resulting increase in the pulmonary arterial pressure leads to right ventricular hypertrophy and eventually death from right heart failure. Excess proliferation of pulmonary arterial endothelial and smooth muscle cells (SMC) is one of the final, common pathological outcomes of distinct pathways involved in the development of IPAH. The pathophysiologic mechanism involves several signaling pathways [1,2], including depolarization and Ca^{2+} overload of the pulmonary arterial SMC (PASMC)[3].

Both the membrane depolarization and the Ca^{2+} overload are the result of altered expression and function of different ion channels and transporters, as well as Ca^{2+} handling proteins. Decreased gene expression or loss-of-function mutation of voltage-gated[4,5] and two-pore domain K^+ channels[6,7], increased expression of nonselective cation channels[8-10], the Na^+/Ca^{2+} exchanger[11], and Ca^{2+} handling proteins[12] have been demonstrated in PASMC of IPAH patients. It has long been known that Ca^{2+} activated Cl^- currents are present in SMC [13], but little attention has been paid to anion channels and transporters in IPAH. Recent reports that identify the encoding genes[14-16] as well as selective blockers of these channels[17,18] provided new tools to assess the role of anion currents in vascular function as well as in pathological states.

The Ca^{2+} activated Cl^- channel TMEM16A, encoded by the gene ANO1, is active at physiological resting membrane potential in human PASMC (approx. -50 mV). Since the intracellular Cl- concentration of a PASMC is relatively high (approx. 45 mM[19]), when TMEM16A channels open, a Cl^- efflux depolarizes the PASMC, with subsequent Ca^{2+} influx. TMEM16A is expressed in the pulmonary arteries of several species including humans[20], but its function in human PASMC and its involvement pulmonary circulatory pathology are poorly understood.

We provide evidence that the expression and function of TMEM16A is significantly increased in IPAH patients, resulting in depolarization and hyperproliferation of PASMCs. Chronic administration of the TMEM16A inhibitor benzbromarone, approved for the treatment of gout in humans, reversed both increased pulmonary arterial pressure and vascular remodeling in animal models of pulmonary hypertension. We present a new approach focusing on the TMEM16A Cl- channel, which might be an important therapeutic target in severe pulmonary hypertension.

These studies have been reported in part in abstract form (References).

Methods

Please see the online supplement for full experimental details, including information on primary human cell isolation, *in vitro* experiments, electrophysiology studies, animal models of pulmonary hypertension and assessment of their endpoints.

Human lung samples

Donor/IPAH patient characteristics are given in Table E1. The clinical trial concerning the acute hemodynamic effects of benzbromarone was registered at https://clinicaltrials.gov/ct2/show/NCT02790450?term=benzbromarone&rank=1 under NCT02790450.

Laser capture microdissection of pulmonary arteries

Laser capture microdissection (LCM) of 17 donor lungs and 14 lungs from IPAH patients was performed as previously described [21].

Animal models of pulmonary hypertension (PH)

All animal studies conformed to the EU guidelines 2010/63/EU and were approved by the University Animal Care Committee; the federal authorities for animal research approved the study protocol (approval numbers: BMWFW-66.010/0144-WF/V/3b/2014, BMWFW-66.010/0076-WF/V/3b/2015).

Statistical analyses

Data are shown either as individual data plots with median, or summarized as mean ± s.e.m. Statistical analyzes were performed using Prism 6.0 (GraphPad Software, La Jolla, CA). Statistical analyses were two-sided for all datasets, and P values <0.05 were considered significant.

Results

Upregulation of TMEM16A in the PASMC of IPAH patients

We tested the expression of anion channels and transporter genes in the laser capture microdissected PA (LCM-PA) of freshly explanted healthy donors and lung recipients suffering from IPAH. The expression pattern of 9 channels and 5 transporters is shown in Figure 1A. The mRNA for the Ca^{2+} activated Cl^- channel TMEM16A gene (*ANO1*) was upregulated in the LCM-PA (Figures 1A and 1B) as well as in primary PASMC isolated from IPAH patients (Figure 1C). No significant regulation of the other channels/transporters was seen, except for the Cl^- channel CFTR, which showed lower expression in the PA of IPAH patients (Figure 1A and E1). Immunofluorescent stainings for α-smooth muscle actin (α-

SMA) and TMEM16A on lung sections of healthy donors and IPAH patients (Figure 1D, Figure E2) showed the presence of TMEM16A in the medial layer of human PA, both in donor lungs and in the remodeled arteries of IPAH lungs, as well as in primary PASMC isolated from both donors and IPAH patients (Figure. E3). Western blots detected a marked increase of TMEM16A in the membrane protein fraction of PASMC from IPAH patients (Figure 1E). Accordingly, whole-cell voltage clamp measurements showed an increased Ca^{2+} activated Cl^- current (I_{ClCa}) in primary PASMC from IPAH patients, compared to the PASMC of healthy donors (Figure 1F).

Next, we addressed upstream events that are likely to regulate TMEM16A. Since the recently reported zinc metalloprotease calcium-activated chloride channel activator 1 (CLCA1) was shown to activate chloride currents in a paracrine fashion and to stabilise cell surface TMEM16A in HEK293T cells exogenously [22,23], we investigated CLCA1 protein levels in the plasma and lungs of IPAH patients. We found that CLCA1 was not significantly altered in plasma and lung homogenate of IPAH patients compared to donors (Figures E4A and E4B). Demographic and hemodynamic data of the patients whose blood plasma or lung homogenate was used for the CLCA1 concentration measurements are shown in Tables E3 and E1, respectively. Treating the PASMC of healthy donors with CLCA1-containing conditioned medium did not affect the resting membrane potential (Figures E4C and E4D). We further quantified the expression of three exons reported to be subject to alternative splicing, since these may influence the biophysical properties of TMEM16A channels. We found no difference in the expression of splice variants between the PASMC of donors and IPAH patients (Figure E5). Accordingly, there was no apparent difference in the biophysical properties of I_{ClCa} in the voltage clamp recordings (Figure 1F and Figure E6). Finally, *in silico* analysis predicted HIF-1α binding sites in the promoter region of the TMEM16A gene. Forty-eight hours of hypoxia increased the amount of TMEM16A protein of the primary PASMC (Figure E7A-B) and formed functional channels in the cell membranes, as demonstrated by an

increased whole-cell current (I_{ClCa}) in the cells exposed to hypoxia (Figure E7C). Thus, in PASMC obtained from healthy donors, chronic hypoxia induced the features of IPAH, including enhanced expression of TMEM16A protein and an increased whole-cell Cl^- current.

Upregulated TMEM16A causes chronic PASMC membrane depolarization in IPAH

In order to detemine the role of TMEM16A in the membrane potential in human PASMC, we controlled the expression of TMEM16A and subsequently examined its impact in human PASMCs. When TMEM16A was silenced, TMEM16A mRNA, total protein and I_{ClCa} in primary PASMC decreased compared to PASMC treated with non-silencing control RNA from donors and IPAH patients (Figures 2A-C, E8, representative current traces shown in Figure E6). Similarly, benzbromarone (BBR), a recently identified inhibitor of TMEM16A channels, significantly decreased whole-cell I_{ClCa} measured in primary PASMC of both donors and IPAH patients (Figure 2D and Figure E6). This BBR-sensitive current was abolished by silencing of TMEM16A (Figure E9). The resting membrane potential (E_m) of primary PASMC isolated from IPAH patients was significantly more depolarized than the E_m of donor PASMC (Figures 2E and 2F). Benzbromarone reversed the E_m of IPAH-PASMC to the levels of PASMC isolated from healthy donors, while it had no effect on the PASMC of donors (Figure 2E). Another structurally non-related TMEM16A blocker, T16Ainh-A01 (abbreviated as T16 in Figure 2E), did not significantly change E_m. Silencing of TMEM16A in IPAH-PASMC rescued (repolarised) the E_m of IPAH-PASMC without significantly affecting donor PASMC (Figure 2F). As a second approach, we overexpressed TMEM16A in human donor PASMC. The overexpression of TMEM16A was verified by an increase in TMEM16A mRNA 48 hrs post-transfection (Figure 2G), and by an increased TMEM16A total protein signal accompanied by an elevated I_{ClCa} (Figures 2H and 2I, respectively). Representative current traces are shown in Supplementary Figure E6). TMEM16A

overexpression brought about a significant depolarization of PASMC, which was reversed by application of BBR (Figure 2J). Note that both the whole-cell I_{ClCa} density and the E_m recorded from the TMEM16A overexpressing donor PASMC mimicked the changes observed in PASMC of IPAH patients.

Acute vasorelaxant effect of the TMEM16A inhibitor benzbromarone

The finding that TMEM16A inhibition reverses membrane depolarization in the PASMC of IPAH patients prompted us to evaluate the effect of TMEM16A inhibition on the pulmonary circulation in both animal models and humans. To determine the effective dose for acute vasorelaxation, we examined the TMEM16A inhibitor mediated PA vasodilator response *ex vivo*. Benzbromarone caused a dose-dependent vasorelaxation of U-46619 preconstricted isolated mouse and rat PA (Figures 3A and 3D). In the second approach we applied benzbromarone *in vivo*. Under continuous *in vivo* hemodynamic monitoring, benzbromarone was applied as an intravenous bolus in two different animal models of PH: in hypoxia-exposed mice (Figures 3B and 3C) and in monocrotaline (MCT)-treated rats (Figures 3E and 3F). Benzbromarone, at a concentration that effectively dilated PAs *ex vivo*, caused a significant decrease in the RVSP in both models without affecting RVSP in the control animals. TMEM16A was not regulated in the heart of PH-animal models (Figure E10). To assess the acute pulmonary vasodilatative potency of benzbromarone in humans, we enrolled 10 patients with severe IPAH and administered 200 mg benzbromarone orally to 8 out of 10 subjects as a single dose during a routine right heart catheter study. Two hundred mg is the maximum approved single oral dose for the preventive treatment of gout in humans. Two patients were excluded - one due to elevated pulmonary arterial wedge pressure (>15mmHg) and another due to elevated serum bilirubin (>1.6 mg/dl). Demographic and hemodynamic data of the patients receiving benzbromarone are described in Table E4. There were no further

changes in the pulmonary or systemic hemodynamics (Table E5). No clinical adverse effects were documented during the study.

Chronic benzbromarone treatment significantly decreases the RVSP and pulmonary arterial muscularization in the hypoxic mouse and monocrotaline rat

To assess the therapeutic potency of benzbromarone for reverse remodeling, we applied benzbromarone and vehicle (Veh) as subcutaneous slow-release pellets in two different animal models of PH. This dosage corresponds to previous studies in models of hyperuricemia in rodents and monkeys [24-26]. A schematic diagram of the experiments using hypoxia-exposed mice is given in Figure 4A and in the Online Methods. RVSP was significantly decreased under long-term benzbromarone treatment, without altering the systemic arterial pressure (SAP). Benzbromarone led to a significant reduction of the hypoxia-induced pulmonary artery muscularization (Figures 4C and 4D).

As in the mouse study, rats were randomized into a control group and two MCT-treated groups (Figure 5A). MCT treatment caused a significant increase in right ventricular free wall (RVFW) thickness and decreases in pulmonary artery acceleration time (PAAT) and cardiac index (CI) as compared to the control group, however, after benzbromarone treatment, there was nearly no effect of MCT, although BBR was only started after two weeks (ns versus control, Figure 5B). Further echocardiographic parameters are reported in Table E6. Compared to the MCT+Veh group, RVSP and RV hypertrophy were significantly decreased in the benzbromarone treated rats (Figure 5C) without changes in SAP. The markedly reduced number of fully muscularized arteries and the increased number of non-muscularized arteries indicated that benzbromarone induced a potent attenuation of vascular remodeling (Figures 5D and 5E).

Upregulated TMEM16A triggers PASMC proliferation

Immunohistological staining of mouse and rat lung sections for the proliferation marker PCNA showed an increased number of PCNA positive nuclei in the medial layer of the PA in both hypoxic mice (Figure 6A) and MCT treated rats (Figures 6B), compared to the normoxic/vehicle-treated controls. In parallel with the hemodynamic improvement, there were fewer PCNA positive nuclei in the BBR-treated animals (Figures 6A and 6B). In human donor and IPAH PASMC, both treatment with BBR and siRNA against TMEM16A led to a decrease in PDGF-BB induced proliferation (Figures 6C -F). We next investigated the direct effect of TMEM16A upregulation on the phosphorylation of c-jun and c-fos (Figure 6). TMEM16A overexpression (Figure 6J) enhanced c-fos phosphorylation, followed by increased PASMC proliferation (Figure 6G-K), which is in line with our previous observation showing increased total c-fos in the remodelled IPAH pulmonary arteries [27]. This suggests that TMEM16A-induced proliferation of human PASMCs is mediated by c-fos phosphorylation and can be inhibited by BBR in both donor and IPAH PASMC (Figures 6L-O).

Discussion

We found increased expression and activation of the Ca^{2+}-activated Cl^- channel TMEM16A in the PASMC of IPAH patients that strongly contributes to the pathologic phenotype of these cells as expressed in depolarization, vasoconstriction and hyperproliferation. Chronic treatment with the TMEM16A inhibitor benzbromarone caused vasodilatation and strong attenuation of remodeling in two independent animal models of PH. Our work also shows that blocking or silencing of TMEM16A reversed the pathological membrane depolarization *in vitro* in the PASMC of IPAH patients, causing vasodilatation, and inhibition of PASMC proliferation.

Our systematic investigation of the compartment-specific regulation of Cl^- channels and transporters in the PA and primary cultured PASMC from IPAH patients showed strongly increased TMEM16A expression. This is in line with other [28-30] reports of upregulation of TMEM16A in the PASMC of animal models of PH. Our study, however, is the first to demonstrate that these changes are very consistent in human PASMC obtained from a large number of IPAH patients. Our study is also the first experimental investigation of the effects of TMEM16A inhibition and overexpression. PASMC isolated from IPAH patients maintained their pathologic phenotype as they were depolarized and showed a TMEM16A upregulation similar to that found in the laser capture microdissected PA. This suggests that the upregulation of TMEM16A is among the pathologic mechanisms of IPAH. This concept is also supported by a previous study showing that endothelin-1 (ET-1), which plays an important role in PAH etiology, upregulates the TMEM16A protein in human PASMC [31]. Moreover, our *in silico* analysis predicted binding sites for the transcription factor HIF1-α in the promoter region of TMEM16A, and a recent study on mouse coronary endothelial cells suggested that hypoxia may increase TMEM16A expression [32]. Accordingly, exposure to hypoxia increased sarcolemmal TMEM16A protein levels in the PASMC of healthy donors with functional consequences due to generation of greater Ca^{2+} activated Cl^- current, compared to PASMC kept under normoxic conditions. Alternative splicing of the TMEM16A mRNA is another way to regulate the biophysical properties of TMEM16A channels: the presence of exons 6b, 13 and 15 is reported to influence Ca^{2+} and E_m sensitivity as well as the speed of channel activation/deactivation [33]. In contrast to the study of Forrest *et al.* in PASMC of monocrotaline treated rats [29], our investigations did not show a differential expression of splice variants between the PASMC of donors and IPAH patients and accordingly, there was no apparent difference in the biophysical properties of the recorded I_{ClCa}. Thus, although there are several potential mechanisms that could upregulate

TMEM16A, a limitation of our study is that it cannot clearly define the signalling pathway leading to TMEM16 overexpression.

The functional consequences of TMEM16A overexpression are summarized in Figure 7. Our electrophysiological studies confirmed previous reports that the PASMC of IPAH patients are significantly depolarized, compared to the PASMC of healthy donors [4]. Moreover, we demonstrated that pharmacological inhibition or silencing of TMEM16A reversed the membrane potential of IPAH-PASMC back to the membrane potential range of healthy donors, whereas overexpression of TMEM16A depolarized the membrane of healthy donors' PASMC to the range of IPAH patients. Since the intracellular Cl^- concentration in SMCs is relatively high [19], the corresponding reverse potential for Cl^- (-25 mV) is higher than the physiological resting membrane potential. Thus, opening of the TMEM16A channels results in Cl^- efflux and subsequent membrane depolarization, opening of the voltage-gated Ca^{2+} channels, Ca^{2+} influx, and consequently PASMC contraction. Benzbromarone has the ability to inhibit URAT1 and xanthine oxidase, therefore it is a well-established medication for the treatment of gout [34]. It has recently been identified as a potent TMEM16A blocker in a multi-drug screening for new TMEM16A inhibitors [18]. We chose benzbromarone in our *ex vivo* and *in vivo* studies because this drug caused an I_{ClCa} inhibition similar to the siRNA treatment against TMEM16A, and its hyperpolarizing effect was similar to the effect of TMEM16A silencing, demonstrating its potency as a TMEM16A channel blocker.

We show that benzbromarone relaxed *ex vivo* pre-constricted mouse PA dose dependently, which is in line with its smooth muscle relaxing properties shown in the bronchi of asthmatic mice [18]. Moreover, we verified the acute hemodynamic effect of benzbromarone *in vivo* in two chronic rodent models of PH. In addition, our current clamp recordings provide evidence that benzbromarone has no effect on the membrane potential of PASMC isolated from healthy donor lungs. This suggests that in the healthy PASMC, this channel is present at low levels with no significant effect on the resting membrane potential

and the resting PA tone. However, its pathologic upregulation and activation induces PASMC membrane depolarization, PA contraction and thereby remodeling. Furthermore, TMEM16A might increase Ca^{2+} sensitivity of the PASMC, as a recent study has found a link between TMEM16A activity and the RhoA/ROCK kinases [35], and it is also known to amplify the store-operated Ca^{2+} entry in human PASMC [36,37].

Oral benzbromarone is approved for preventive treatment of gout. In a pilot study in 10 IPAH patients undergoing right heart catheterisation, we applied a single maximal approved dose, but did not observe any acute vasodilatory effects. The lack of any acute effect was probably due to low benzbromarone plasma concentrations and a very short exposure time. ET-1 receptor blockers, for example, although clinically highly effective, also have no acute hemodynamic effects. Chronic administration of benzbromarone corresponding to therapeutic doses in models of hyperuricemia in rodents or monkeys [24-26] improved the PH phenotype in two different rodent models. Our hemodynamic and echocardiographic data show that four weeks after PH induction, in the hypoxic mouse model and in the monocrotaline rat model, benzbromarone significantly attenuated the deleterious effects on RVFW thickness, CI, PAAT, RVSP, and Fulton index partly indiscernable from control levels. This suggests that benzbromarone had strong beneficial effects on the pulmonary vascular remodeling. The most likely molecular mechanism is the inhibition of TMEM16A by benzbromarone. As a limitation of the study, we cannot exclude that the in vivo efficacy of BBR was in part mediated through effects on other pathways such as URAT1 and xanthine oxidase. However, we provide specific evidence for the TMEM16A pathway by the TMEM16A silencing and overexpression experiments in human PASMC. Indeed, the TMEM16A overexpression mimicked the features of IPAH PASMC, showing significantly increased PASMC proliferation via c-fos phosphorylation.

In conclusion, we found that the Ca^{2+}-activated Cl^- channel TMEM16A is importantly involved in the pathologic mechanisms leading to chronic PASMC depolarization,

vasoconstriction and proliferation, all important features of IPAH. As a proof of principle, we demonstrated that TMEM16A inhibition by chronic benzbromarone application strongly attenuates remodeling in two different rodent models of PH, suggesting that TMEM16A is an important novel drug target for treatment of PAH.

Acknowledgements

We are grateful to Dr. Elvira Stacher and Dr. Zoltan Balint who gave us valuable input on the design and execution of experiments, Eugenia Lamont, BA for proof reading the manuscript. The excellent technical help of Simone Tischler, Elisabeth Blanz, Sabine Halsegger, Lisa Oberreiter, Ida Niklasson and Verena Braunschmid are appreciated. Funding acknowledgement: D.S.M. was supported by the PhD programm from the Medical University of Graz DK-MOLIN. N.S. was supported by the Molmed PhD programm of the Medical Uiversity of Graz.

Main Figure Legends

Figure 1. Upregulation of TMEM16A and increased I_{ClCa} in the PASMC of IPAH patients.

(A) qRT-PCR heat map depicting the expression of 9 Cl^- channel and 5 Cl^- transporter genes in laser capture microdissected pulmonary arteries (LCM-PA) of 17 healthy donors and 14 IPAH patients. ΔCt values, calculated by normalizing the expression of target genes to β2 microglobulin expression, are shown. White boxes indicate that no PCR product was detected. **(B, C)** Expression of the TMEM16A mRNA in LCM-PA **(B)** and in primary PASMC **(C)** isolated from donors (n=7-15) and IPAH (n=7-16) patients. ΔCt values have been calculated as the difference of TMEM16A and β2 microglobulin expression. **(D)** Immunofluorescence staining for α smooth muscle actin (α-SMA) and TMEM16A on lung sections of donors and IPAH patients. Scale bar, 50 µm. **(E)** Western blot comparing cell membrane expression of TMEM16A in the PASMC of donors (n=4) and IPAH patients (n=4). Membrane and cytosolic protein fractions were separated by cell surface protein biotinylation. The Na^+-K^+ ATPase α1 subunit (NKA α1) and α-tubulin served as loading controls for membrane and cytosolic fractions, respectively. **(F)** Representative whole-cell Ca^{2+} activated Cl^- current (I_{ClCa}) traces and normalized current-voltage (I-V) relationships measured with voltage clamp in the PASMC of healthy donors and IPAH patients (n=10 for donors and n=9 for IPAH). ** $p < 0.01$, *** $p < 0.001$, unpaired t test used in **B, C** and **E**. Two-way-ANOVA with Bonferroni post test was used in **F**. Figure C-F were performed with 4-7 different donor or IPAH patients.

Figure 2. TMEM16A influences membrane potential in human PASMC.

(A, B) TMEM16A mRNA expression **(A)** and total protein level **(B)** in PASMC treated with either non-silencing control RNA (NS) or TMEM16A siRNA (SI). mRNA expression was studied 48 hours post-transfection and is given as ΔCt, calculated as the difference of TMEM16A and β2 microglobulin expression. **(C)** I_{ClCa} density in the PASMC of IPAH patients 72 hours after treatment with non-silencing control RNA (NS, n=9) or TMEM16A siRNA (SI, n=7). **(D)** Effect of benzbromarone (BBR, 30 µM) on I_{ClCa} density in the PASMC of IPAH patients (IPAH n=9, IPAH+BBR n=7). **(E)** Membrane potential (E_m) values obtained from PASMC of healthy donors (n=7-18) and IPAH patients (n=8-23) in the absence or presence of the TMEM16A blockers $T16A_{inh}$-A01 (T16Ainh, 10 µM) or benzbromarone (BBR, 30 µM). **(F)** Membrane potential (E_m) of PASMC 72 hrs after transfection with either non-silencing control RNA (NS) or siRNA against TMEM16A (SI). **(G, H)** TMEM16A mRNA **(G)** and protein **(H)** expression in donor PASMC (n=4) after transfection with TMEM16A gene (*ANO1*) -containing or empty pQCXIP plasmide (labeled as pQCXIP-ANO1 and pQCXIP, respectively). **(I)** I_{ClCa} I-V curves measured in the PASMC of donors 72 hours after transfection with empty (n=6) or TMEM16A gene (*ANO1*) -containing (n=8) pQCXIP plasmide. **(J)** Effect of transfection with empty or TMEM16A gene containing pQCXIP plasmide on the membrane potential (E_m) of PASMC isolated from donors (n=6-7). * $p < 0.05$, ** $p < 0.01$, *** $p < 0.001$, unpaired t test was used in **A and G** , two-way ANOVA with Bonferroni post-hoc test in **C, D, I** and **J**, and one-way ANOVA with Bonferroni's Multiple Comparison Test in **E** and **F**. All experiments in Figure 2 were performed with 4-8 different donor or IPAH patients.

Figure 3. Acute TMEM16A inhibition relaxes the PA both *ex vivo* and *in vivo.*

Effect of the TMEM16A blocker benzbromarone (BBR) applied in cumulative doses on U-46619 (30 nM) preconstricted mouse (A) and rat (D) pulmonary artery rings. **(A)** Representative traces, **(B)** Dose-response curves from mouse (n=7) (A) and rat (n=4) pulmonary artery rings. **(B, C)** Pre- and postdrug values **(B)** and maximal changes **(C)** in RVSP measured with *in vivo* hemodynamics during a single i.v. administration of 300 µM BBR in mice exposed to 4 weeks of hypoxia or normoxia. **(E, F)** Pre- and postdrug values **(E)** and maximal changes **(F)** in RVSP measured by means of *in vivo* hemodynamics during a single i.v. administration of 300 µM BBR in rats treated with monocrotaline (MCT) or vehicle. ** $p < 0.01$, *** $p < 0.001$, two-way ANOVA with Bonferroni post test in **B** and **E**, unpaired t test in **C** and **F**. $^{\#}$ $p < 0.05$, $^{\#\#\#}$ $p < 0.001$, unpaired t test in **B** and **E**.

Figure 4. Chronic treatment with the TMEM16A inhibitor benzbromarone reverses vasoconstrictive PA remodeling in mice exposed to hypoxia.

(A) Schematic diagram of the experimental protocol. Mice were randomized into three groups. Groups HOX+Veh and HOX+BBR were exposed to 4 weeks of hypoxia, while mice in the control group (n=8) were kept under normoxic condictions. After week 2, subcutaneous slow-release pellets containing either vehicle (HOX+Veh group, n=8) or benzbromarone (HOX+BBR, n=8) were implanted. At week 4, mice underwent hemodynamic analyses and were sacrificed for organ collection, as indicated in the figure. **(B)** Assessment of RVSP with *in vivo* hemodynamics and estimation of right ventricular hypertrophy (Fulton-index). **(C)** Analysis of pulmonary arterial remodeling expressed as the percentage change in the number of muscularized and non-muscularized arteries (Control n=3, HOX+Veh n=5, HOX+BBR n=5). **(D)** Representative images showing the degree of muscularization of resistance size arteries. Scale bar, 50 µm. ** $p < 0.01$, *** $p < 0.001$, one-way ANOVA with Bonferroni's Multiple Comparison Test was used in **B** and **C**.

Figure 5. Chronic treatment with the TMEM16A inhibitor benzbromarone reverses vasoconstrictive PA remodeling in monocrotaline treated rats.

(A) Schematics of the experimental protocol. Rats were randomized into three groups. Groups MCT+Veh and MCT+BBR (n=8 each) were treated with monocrotaline (MCT), while rats in the control group (n=8) received vehicle. Two weeks after MCT treatment, subcutaneous slow-release pellets containing either vehicle (MCT+Veh group) or benzbromarone (MCT+BBR) were implanted. At week 4, all rats were subjected to hemodynamic analyses and organ collection, as indicated. **(B)** Echocardiographic assessment of the right ventricular free wall (RVFW) thickness, cardiac index (CI), and pulmonary artery acceleration time (PAAT) at week 4, one day before termination of the experiment. **(C)** RVSP measured by *in vivo* hemodynamics and calculation of right ventricular hypertrophy (Fulton-index). **(D)** Analysis of pulmonary arterial remodeling expressed as percentage change in the number of muscularized and non-muscularized arteries (Control n=4, MCT+Veh n=7, MCT+BBR n=5). **(E)** Representative images showing the degree of muscularization of resistance arteries. Scale bar, 50 µm. * $p < 0.05$, ** $p < 0.01$, *** $p < 0.001$, one-way ANOVA with Bonferroni's Multiple Comparison Test in **B, C** and **D**.

Figure 6. Role of TMEM16A in the proliferation of human PASMC.

(A) PCNA staining (brown) of the PA in mice that underwent 4 weeks of hypoxia and were treated either with vehicle or benzbromarone throughout weeks 3 and 4, compared to untreated normoxic controls. Scale bar, 50 µm. **(B)** PA of control as well as MCT treated rats that received either vehicle or benzbromarone throughout week 3 and 4 after MCT treatment, stained for PCNA (brown). Scale bar, 50 µm. **(C, D)** PDGF-BB induced proliferation of human donor and IPAH PASMC, measured with thymidine incorporation, in the absence (Veh) or presence of 30 µm benzbromarone (BBR, n=6 in all groups). Changes are expressed as percentage change compared to the untreated controls (Ctrl). **(E, F)** PDGF-BB induced

proliferation of human donor and IPAH PASMC, measured with thymidine incorporation, 72 hours after treatment with either non-silencing control RNA (NS) or TMEM16A siRNA (SI, n=6 in all groups). Changes are expressed as percentage change compared to the controls treated with non-silencing control RNA only (NS). * $p < 0.05$, ** $p < 0.01$, *** $p < 0.001$, one-way ANOVA with Bonferroni's Multiple Comparison Test. (G) Representative western blots of PASMCs overexpressing CTL-plasmid or TMEM16A plasmid blotted for TMEM16A, phosphroylated and total cfos and cjun and GAPDH. (H-J) Summarized western blot data of n =7. (K) Overexpression of TMEM16A increased proliferation in PASMCs under basal conditions (n=8), measured with thymidine incorporation. Changes are expressed as percentage change compared to the controls (CTL-AV). Representative western blots of Donor (L) and IPAH (M)PASMCs treated with or without BBR (30µM) blotted for TMEM16A, phosphroylated and total cfos and GAPDH. (N-O) Summarized western blot data of n =7.* $p < 0.05$, ** $p < 0.01$ unpaired T-Test.

Figure 7. Effect of TMEM16A upregulation on the resting membrane potential in human PASMC and its pathophysiological consequences.

The membrane potential (E_m) of the PASMC is the key to determining the intracellular Ca^{2+} concentration $[Ca^{2+}]_i$ and the function of the PA. The E_m of a healthy PASMC is around -50 mV. Only a few TMEM16A channels are present and are not activated. Due to the negative E_m, voltage-gated Ca^{2+} channels (VGCC) are closed, and $[Ca^{2+}]_i$ is low. In contrast, the overexpression and increased activation of TMEM16A channels represent a depolarizing current, raising E_m to around -30 mV. The subsequent VGCC opening increases $[Ca^{2+}]_i$, leading to PA contraction and PASMC proliferation. In addition, TMEM16A causes hyperproliferation via c-fos phosphorylation.

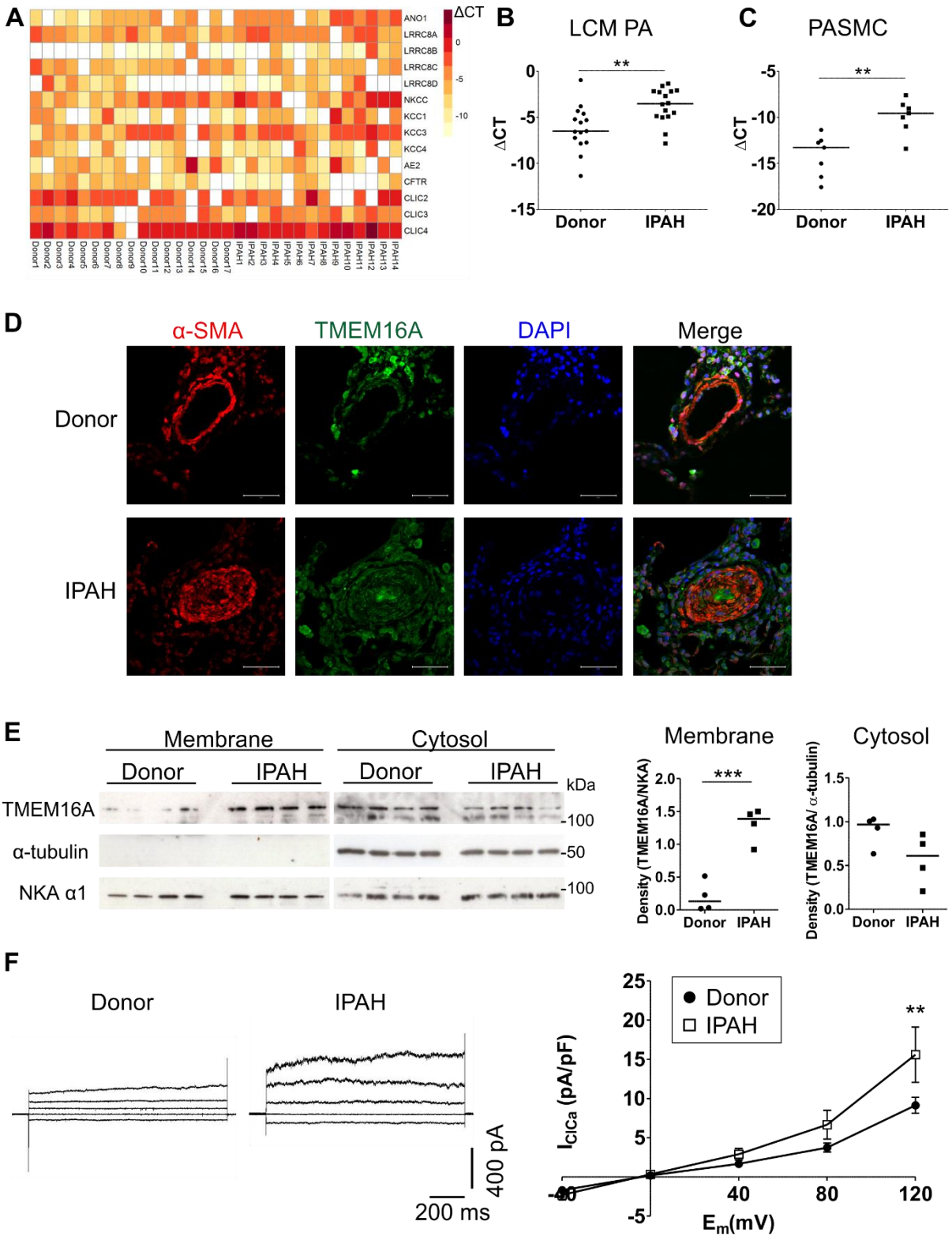
A
ΔCT
ANO1
LRRC8A
LRRC8B
LRRC8C
LRRC8D
NKCC
KCC1
KCC3
KCC4
AE2
CFTR
CLIC2
CLIC3
CLIC4
B
LCM PA
ΔCT
Donor
IPAH
C
PASMC
ΔCT
Donor
IPAH
D
α-SMA
TMEM16A
DAPI
Merge
Donor
IPAH
E
Membrane
Cytosol
Donor
IPAH
Donor
IPAH
kDa
TMEM16A
α-tubulin
NKA α1
-100
-50
-100
Membrane
Density (TMEM16A/NKA)
Donor
IPAH
Cytosol
Density (TMEM16A/ α-tubulin)
Donor
IPAH
F
Donor
IPAH
400 pA
200 ms
Donor
IPAH
I_ClCa (pA/pF)
E_m(mV)

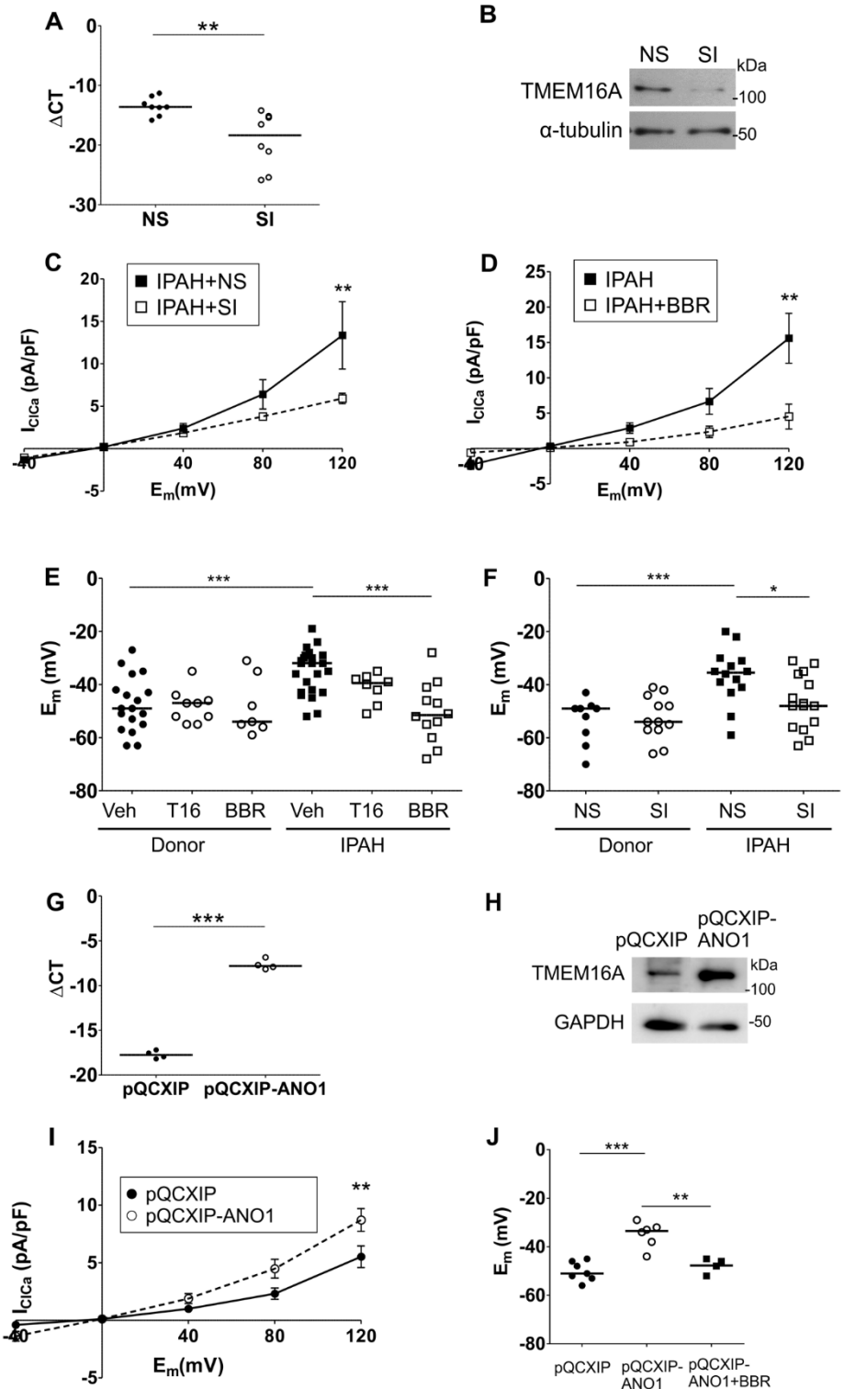
A
**
ΔCT
0
-10
-20
-30
NS
SI
B
NS
SI
kDa
TMEM16A
-100
α-tubulin
-50
C
IPAH+NS
IPAH+SI
**
I_ClCa (pA/pF)
20
15
10
5
-5
40
80
120
E_m(mV)
D
IPAH
IPAH+BBR
**
I_ClCa (pA/pF)
25
20
15
10
5
-5
40
80
120
E_m(mV)
E
***
***
E_m (mV)
0
-20
-40
-60
-80
Veh
T16
BBR
Veh
T16
BBR
Donor
IPAH
F
***
*
E_m (mV)
0
-20
-40
-60
-80
NS
SI
NS
SI
Donor
IPAH
G
***
ΔCT
0
-5
-10
-15
-20
pQCXIP
pQCXIP-ANO1
H
pQCXIP
pQCXIP-ANO1
TMEM16A
kDa
-100
GAPDH
-50
I
pQCXIP
pQCXIP-ANO1
**
I_ClCa (pA/pF)
15
10
5
-5
40
80
120
E_m(mV)
J
***
**
E_m (mV)
0
-20
-40
-60
-80
pQCXIP
pQCXIP-ANO1
pQCXIP-ANO1+BBR

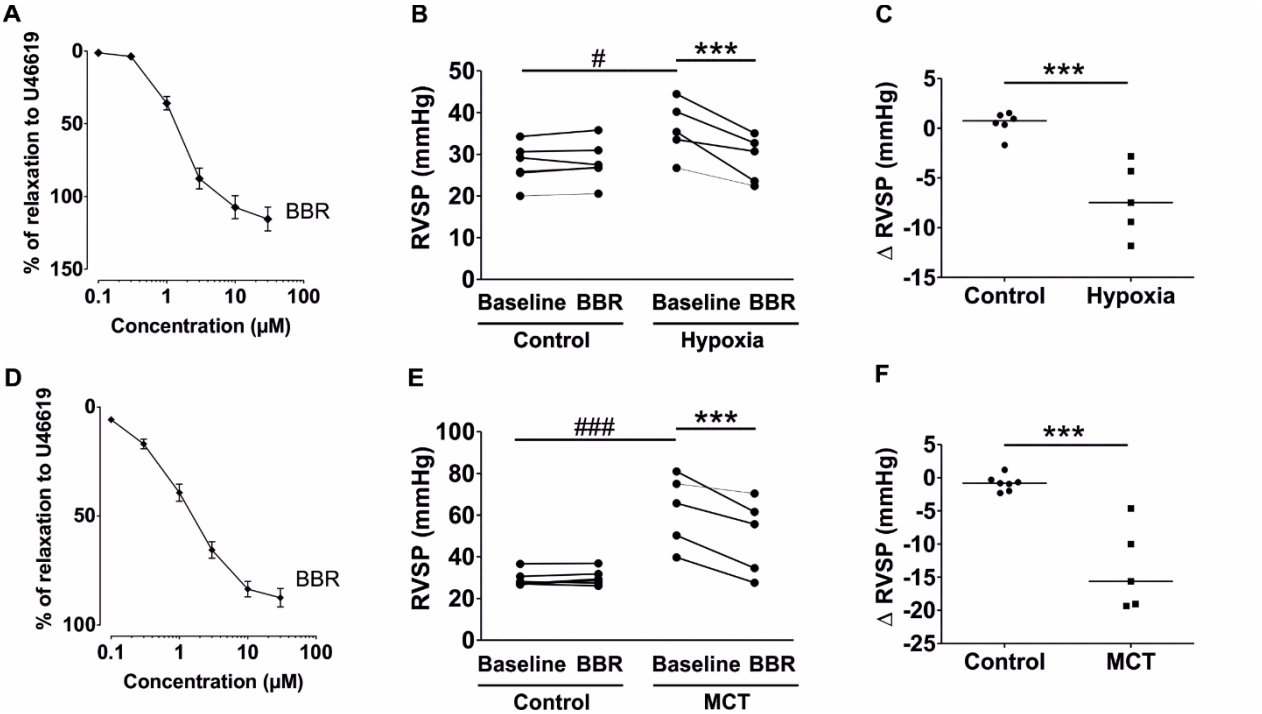
A
% of relaxation to U46619
0
50
100
150
BBR
0.1
1
10
100
Concentration (μM)
B
RVSP (mmHg)
#
***
Baseline BBR
Baseline BBR
Control
Hypoxia
C
Δ RVSP (mmHg)
***
Control
Hypoxia
D
% of relaxation to U46619
BBR
Concentration (μM)
E
RVSP (mmHg)
###
***
Baseline BBR
Baseline BBR
Control
MCT
F
Δ RVSP (mmHg)
***
Control
MCT

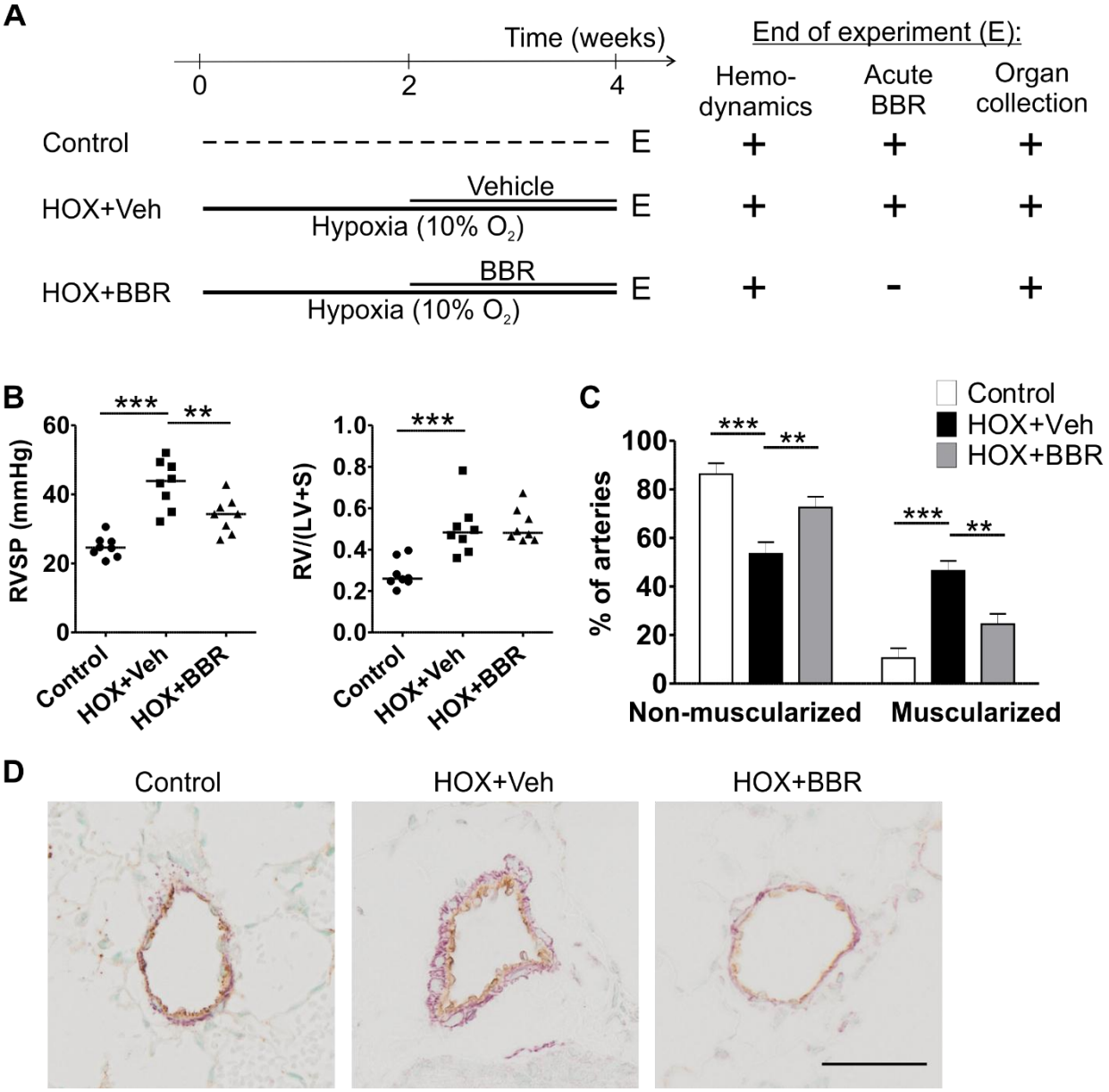
A
Time (weeks)
0
2
4
End of experiment (E):
Hemo-dynamics
Acute BBR
Organ collection
Control
E
+
+
+
HOX+Veh
Vehicle
Hypoxia (10% O2)
E
+
+
+
HOX+BBR
BBR
Hypoxia (10% O2)
E
+
-
+
B
RVSP (mmHg)
60
40
20
0
***
**
Control
HOX+Veh
HOX+BBR
RV/(LV+S)
1.0
0.8
0.6
0.4
0.2
0.0
***
Control
HOX+Veh
HOX+BBR
C
Control
HOX+Veh
HOX+BBR
% of arteries
100
80
60
40
20
0
***
**
***
**
Non-muscularized
Muscularized
D
Control
HOX+Veh
HOX+BBR

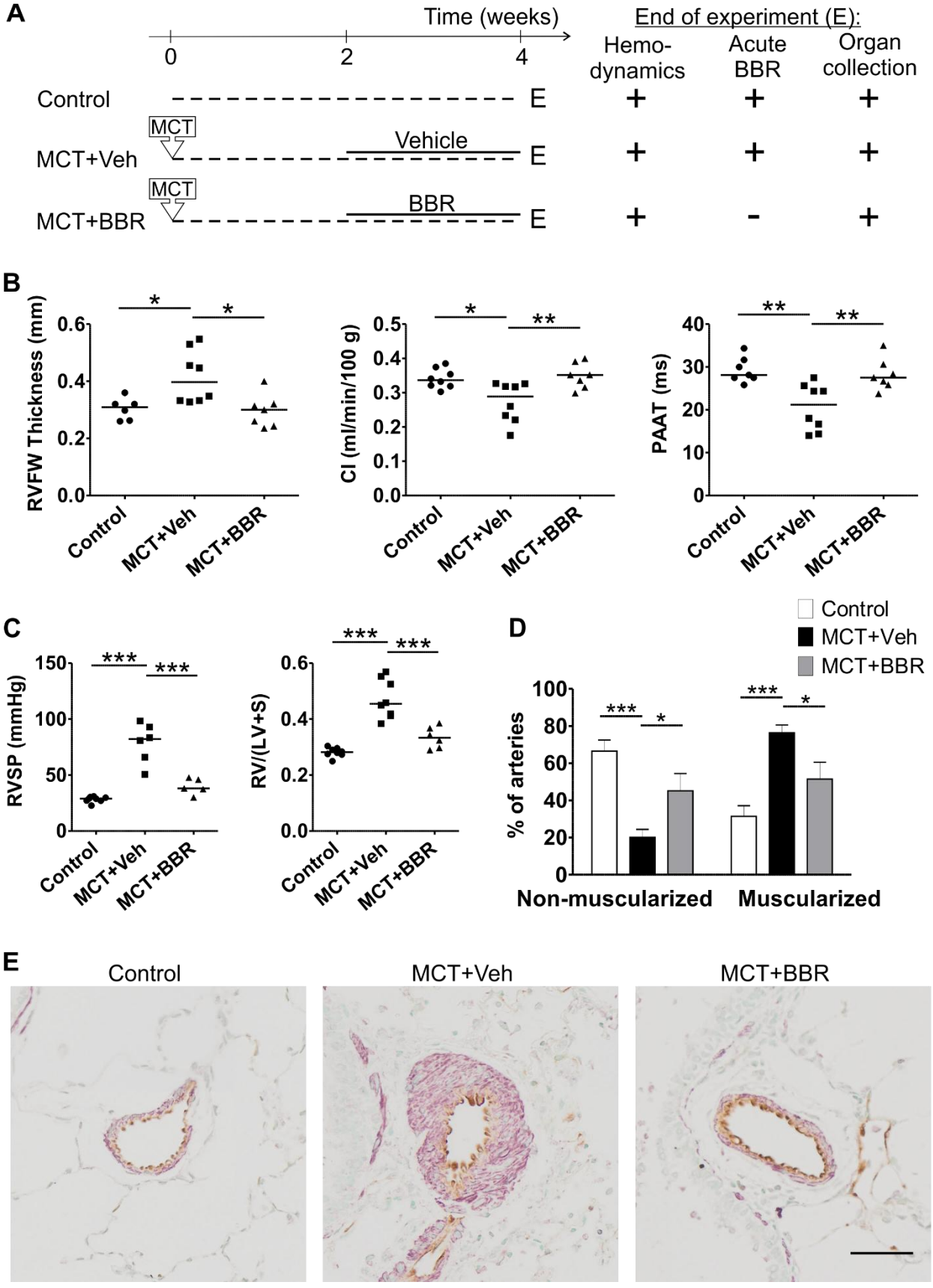
A
Time (weeks)
0
2
4
End of experiment (E):
Hemo-dynamics
Acute BBR
Organ collection
Control
E
+
+
+
MCT
Vehicle
MCT+Veh
E
+
+
+
MCT
BBR
MCT+BBR
E
+
-
+
B
RVFW Thickness (mm)
CI (ml/min/100 g)
PAAT (ms)
Control
MCT+Veh
MCT+BBR
C
RVSP (mmHg)
RV/(LV+S)
D
Control
MCT+Veh
MCT+BBR
% of arteries
Non-muscularized
Muscularized
E
Control
MCT+Veh
MCT+BBR

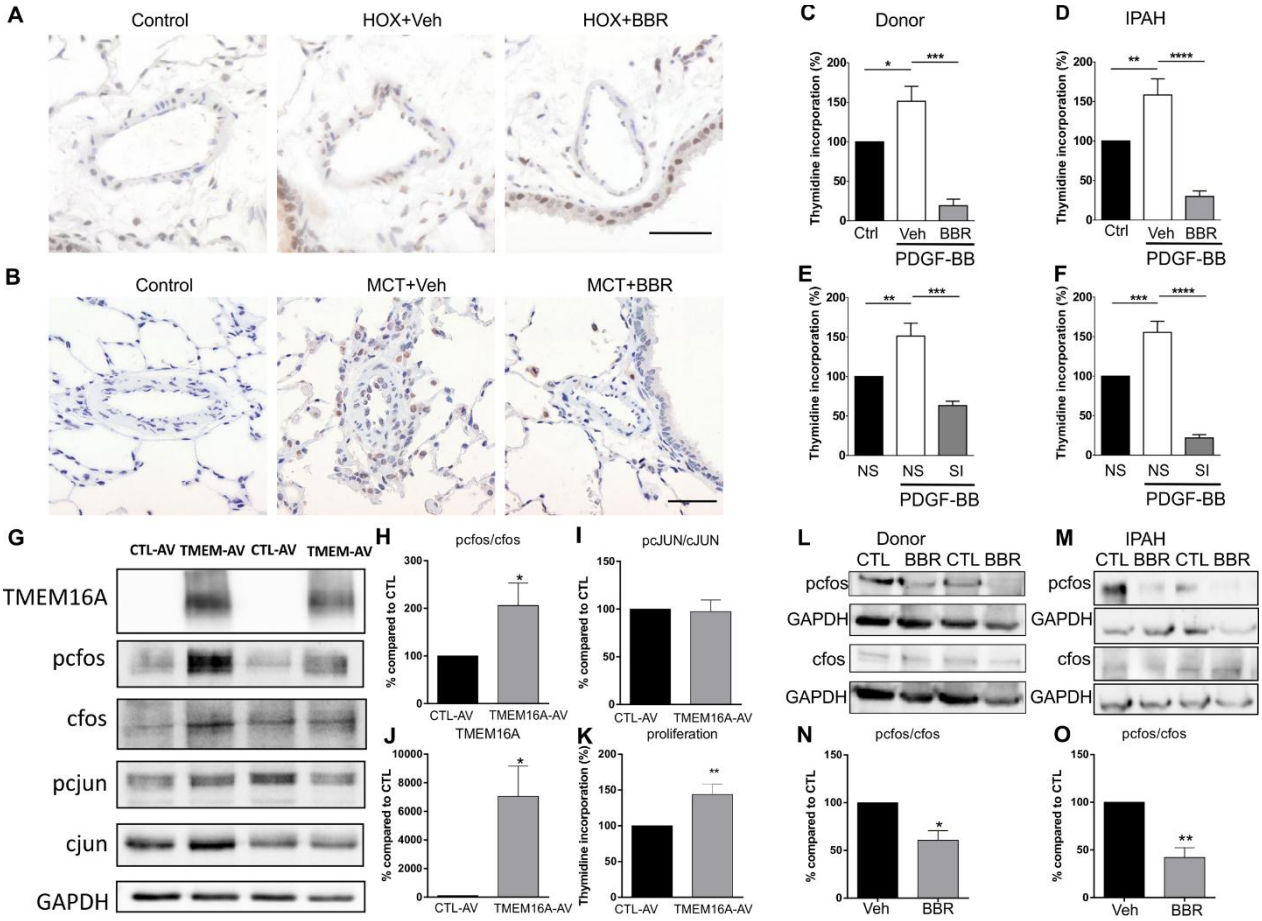
A
Control
HOX+Veh
HOX+BBR
B
Control
MCT+Veh
MCT+BBR
C
Donor
Thymidine incorporation (%)
Ctrl
Veh
BBR
PDGF-BB
D
IPAH
E
NS
NS
SI
F
G
CTL-AV
TMEM-AV
CTL-AV
TMEM-AV
TMEM16A
pcfos
cfos
pcjun
cjun
GAPDH
H
pcfos/cfos
% compared to CTL
I
pcJUN/cJUN
J
TMEM16A
K
proliferation
L
Donor
CTL
BBR
CTL
BBR
M
IPAH
N
pcfos/cfos
Veh
BBR
O
pcfos/cfos

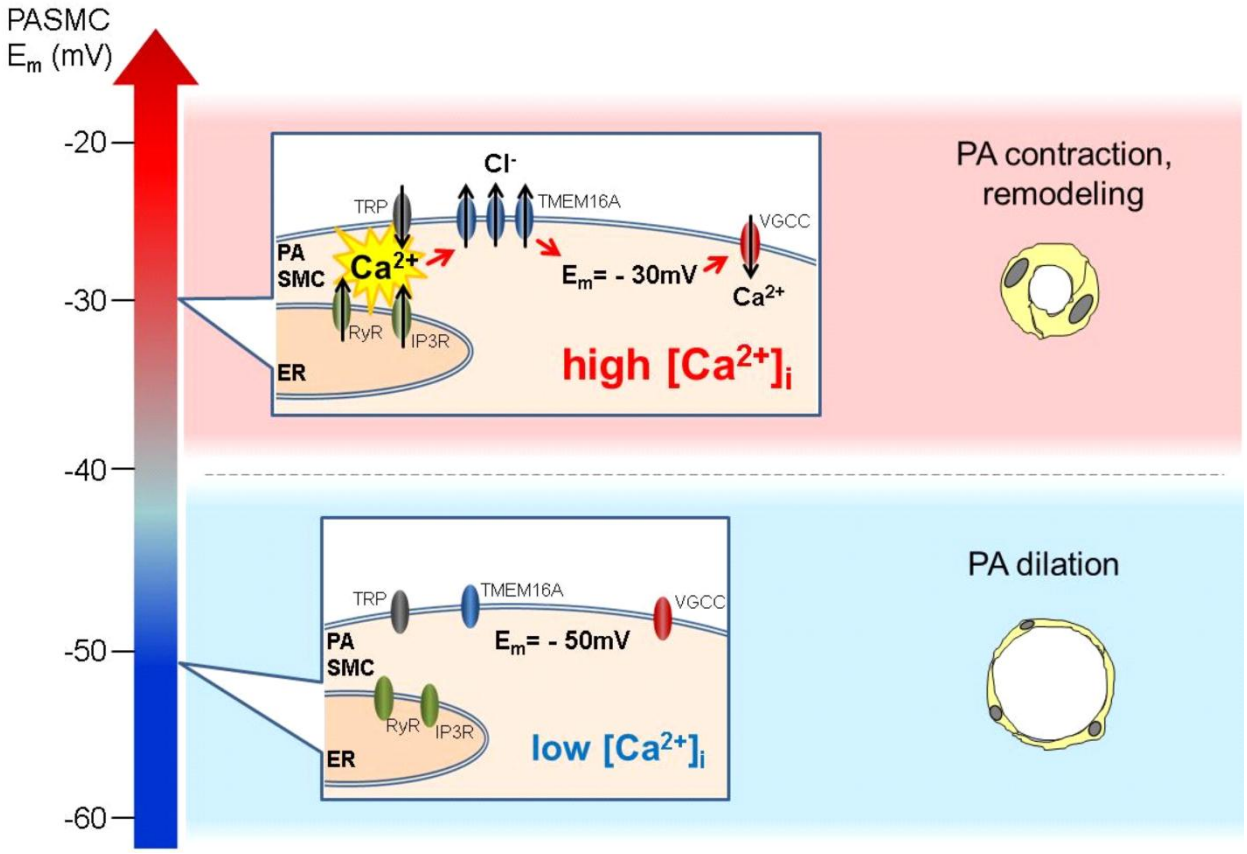
PASMC
E_m (mV)
-20
-30
-40
-50
-60
Cl^-
TRP
TMEM16A
VGCC
PA
SMC
Ca^{2+}
E_m= - 30mV
Ca^{2+}
RyR
IP3R
ER
high $[Ca^{2+}]_i$
PA contraction,
remodeling
TRP
TMEM16A
VGCC
PA
SMC
E_m= - 50mV
RyR
IP3R
ER
low $[Ca^{2+}]_i$
PA dilation

S

Online Supplementary Material

Supplementary Methods

Human lung samples

Human lung tissue samples were obtained from patients with idiopathic pulmonary arterial hypertension (IPAH) who underwent lung transplantation at the Department of Surgery, Division of Thoracic Surgery, Medical University of Vienna, Vienna, Austria. The protocol and tissue usage were approved by the institutional ethics committee (976/2010) and written patient consent was obtained before lung transplantation. The patient characteristics included: age at the time of the transplantation, weight, height, sex, mean pulmonary arterial pressure (mPAP) measured by right heart catheterization, pulmonary function tests, as well as the medical therapy. The chest computed tomography (CT) scans and right heart catheterization (RHC) data were reviewed by experienced pathologists and pneumologists to verify the diagnoses. Healthy donor lung tissue was obtained from the same source. Donor/IPAH patient characteristics are given in Table E1.

The clinical trial concerning the acute hemodynamic effects of benzbromarone was registered at https://clinicaltrials.gov/ct2/show/NCT02790450?term=benzbromarone&rank=1 under NCT02790450.

Laser capture microdissection of pulmonary arteries

Laser capture microdissection (LCM) of 17 donor lungs and 14 lungs from IPAH patients, as well as mRNA subtraction and cDNA preparation were performed as previously described(1). The intima and media layers of pulmonary arteries of 100-500 μm diameter were collected.

Primary human pulmonary arterial smooth muscle cell (PASMC) isolation

The isolation and culture of PASMC has been performed according to Stulnig *et al* (2). VascuLife Complete SMC Medium (LifeLine Cell Technology, Frederick MD, USA) containing 10% FCS (Biowest, Nuaillé, France) and 0.2% antibiotics/antimycotics (LifeLine Technology) was used for culturing. Immunofluorescent labelings (described in details below)

were performed routinely on these cells to test for α-smooth muscle actin positivity and the lack of signal for von Willebrand factor. For all experiments, PASMC underwent no more than one freeze/thaw cycle (freezing medium: VascuLife Complete SMC Medium containing 15% FCS and 10% DMSO) and cells were used no longer than the 5th passage. Age, sex and mPAP (if known) of the donors and IPAH patients from which PASMC were isolated are reported in Table E1.

qRT-PCR

Laser capture microdissected human pulmonary arteries

The expression of ion channels and transporters was analyzed with qRT-PCR using the QuantiFast SYBR PCR reagent (Qiagen, Hilden, Germany). Primer pairs (Eurofins, Graz, Austria), summarized by Table E2, were designed to span at least one exon-exon boundary to avoid the amplification of genomic DNA. The specificity of all primers as well as the legth of the amplicon were confirmed by melting curve analysis and by running the products on 2% agarose gels, respectively. Expression levels (confirmed by melting curve analysis and by running the products on 2% agarβ_2-microglobulin and the Ct of the target genes

Primary human pulmonary arterial smooth muscle cells

PASMC were grown until confluence, serum-starved overnight using VascuLife Basal Medium containing 0.2% antibiotics, then RNA was isolated using the PeqGOLD Total RNA kit (PeqLab, Erlangen, Germany) and transcribed into cDNA with the iScript reagent mix (Bio-Rad, Hercules CA, USA). qRT-PCR was performed as described above. To assess *ANO1* expression, the primers targeted the boundary of exons 1 and 2. As this region is not reported to be subject of alternative splicing, these primers amplified all splice variants. In order to study alternative splicing, primer design principles are depicted in Figure E4a. Exon detecting ("detect") primers were designed so that one of the primers should attach to the

studied exon. Primers detecting the absence of an exon ("missing") were created so that one of the primers should bind to the corresponding exon-exon boundary only when the studied exon is missing.

Immunofluorescence staining for TMEM16A

Formalin-fixed paraffin-embedded human lung tissue blocks were cut to 3.5 µm thick sections and antigen retrieval was performed with Dako Target Retrieval Solution pH 9.0 (Dako, Glostrup, Denmark) at 95^{0}C. After blocking with 3% BSA, sections were immunolabeled for α-smooth muscle actin (EB06450, Everest Biotech, Upper Heyford, UK) and TMEM16A (#ACL-011, Alomone Labs, Jerusalem, Israel) overnight, followed by a labeling with Alexa Fluor 488 conjugated anti-rabbit and Alexa Fluor 555 conjugated anti-goat secondary antibodies (Life Technologies, Carlsbad CA, USA). Slides were covered using Vectashield mounting medium with DAPI (Vector Laboratories, Peterborough, UK) and imaged with a Zeiss LSM 510 META laser scanning confocal microscope. Duplicates were processed without the primary antibody and/or with the primary antibody pre-incubated with the immunogen peptide as negative controls (Figure E1).

PASMC seeded on chamber slides were fixed with formalin, permeabilized with 0.1% Triton X-100 and then processed the same way as reported for the formalin-fixed lung tissue. Images together with negative controls are shown in Supplementary Figure E2.

Analysis of protein expression

Human PASMC sarcolemmal proteins

Human PASMC grown on 10 cm Petri dishes were labeled with 1 mg/ml EZ-link NHS-SS-biotin (Thermo Scientific, Waltham MA, USA) for 1 h at 4 °C and rinsed 3 times with PBS (137 mM NaCl, 2.7 mM KCl, 10 mM Na2HPO4, 2 mM KH2PO4, pH 7.4) containing 100 mM glycine. Cells were then solubilized in cell lysis buffer (50 mM Tris pH 7.4, 100 mM

NaCl, 50 mM NaF, 5 mM β-glycerophosphate, 2 mM EDTA, 2 mM EGTA, 1 mM sodium orthovanadate, 0.1 % Triton X-100) containing protease inhibitor cocktail (Roche Diagnostics, Basel, Switzerland). Protein concentration was determined using a Pierce BCA Protein Assay Kit (Thermo Scientific). 100 µg of protein per sample were incubated overnight at 4°C with end-over-end shaking in the presence of Neutravidin Agarose Resin Beads (Thermo Scientific). After centrifugation, the supernatant was carefully removed from the beads and frozen as the cytosolic fraction. In order to purify the membrane protein fraction, beads were washed and resuspended in 25 µl of 2x Laemmli sample buffer (10% SDS, 20% Glycerol, 0.2 M Tris-HCl, 0.05% bromophenol blue, 10% beta mercaptoethanol). Biotinylated cell surface proteins as well as the cytosolic fractions were separated on a 10% SDS-PAGE, followed by electrotransfer to a PVDF membrane (GE Healthcare, Little Chalfont, UK). After blocking the membrane with 5 % non-fat milk in TBS-T (5 mM Tris-Cl, 150 mM NaCl, 0.1% Tween 20, pH 7.5), the membrane was labeled for TMEM16A (ab53212, Abcam, Cambridge, UK), followed by incubation with horseradish peroxidase conjugated secondary antibody (Dako, Glostrup, Denmark). Final detection of the proteins was performed using an ECL Plus Kit (GE Healthcare, Little Chalfont, UK) and a ChemiDocTM Touch Imaging System. To verify the purity of the membrane fraction and to determine the amounts of protein loaded on the gel, blots were stripped with RestoreTM Plus Western Blot Stripping Buffer (Thermo Scientific) and reprobed using antibodies against NA/K ATPase (ab 74945), LRP-1 (ab92544, both from Abcam),α-tubulin (11H10 Cell Signaling Technology - New England Biolabs, Hitchin, UK), pp38 (#9211S), p38 (9212S), pERK (#9101S), ERK (#9102S), pcFos (#5348P), cFos (#4384S), pcJun (#3270P), cJun (#9165P) from Cell Signaling Technology, Danvers, MA, USA or GAPDH (sc25778, Santa Cruz Biotechnology, Dallas, Texas, USA).

Human PASMC total protein

Human PASMC were grown on 6-well plates until confluence, serum-starved overnight, and harvested using RIPA buffer (Sigma) supplemented with protease inhibitors (Roche). The cell lysate was sonicated and centrifuged for 10 min at 5000 g. Protein concentration of the supernatant was determined using the Pierce BCA Protein Assay Kit (Thermo Scientific), then 20 µg protein from each sample was mixed with 10x Laemmli sample buffer and ran on 10% SDS-PAGE. Transfer, immunolabeling and signal detection were carried out as described above.

Manipulation of TMEM16A expression

For TMEM16A silencing, human PASMC were serum-starved for 3 hours, then transfected either with 100 nM siRNA against TMEM16A (SMART Pool: ON-TARGET plus ANO1 siRNA, Cat # L-027200-00-0005, Dharmacon, Lafayette Co, USA) or with non-silencing control RNA (ON-TARGET plus Non-targeting pool, Cat # D-001810-10-05, Dharmacon) using the Effectene transfection reagent kit (Qiagen) in serum-free medium. After 6 hours, the reagent mixture was replaced with Complete SMC Medium. We observed a significant reduction of the TMEM16A mRNA and protein 48 and 72 hours post-transfection, respectively (Figure 2A and 2B). Similarly, 72 hours post-transfection a significant decrease in I_{ClCa} was observed (Figure 2C).

The vector used for TMEM16A overexpression was constructed at the University of Münster, by cloning the TMEM16A gene from a human podocyte cDNA library into a pQCXIP expression plasmid. Transfection was performed in Complete SMC Medium overnight, following the instructions of the Effectene transfection reagent kit (Qiagen), then the reagent mixture was changed to Complete SMC Medium. As a control, cells from the same batch were transfected with the empty pQCXIP plasmid. A significant elevation in the TMEM16A

mRNA was observed 48 hours post-transfection (Figure 2G), accompanied by an increased TMEM16A protein level and I_{ClCa} density 72 hours post-transfection (Figure 2H and I).

Electrophysiology

Membrane potential (E_m) measurement

PASMC were grown on glass coverslips and serum starved for 24-48 hours. The coverslips were perfused with a bath solution composed of (in mM) NaCl 141, KCl 4.7, HEPES 10, glucose 10, CaCl2 1.8, MgCl2 1.2, pH 7.4 (NaOH) at room temperature. Micropipettes were pulled of borosilicate glass capillaries (GC150F-10, Harvard Apparatus Ltd, Edenbridge, Kent, UK) with a P-2000 electrode puller (Sutter Instruments, Novato Ca, USA), and fire polished using a micro-forge (MF-830, Narishige,Tokyo, Japan) to give a final resistance of 3-5 MΩ when filled with the pipette solution (composition in mM: NaCl 10, KCl 125, K2ATP 5, HEPES 10, EGTA 5, MgCl2 4, pH set to 7.2 with KOH). E_m was measured with a HEKA EPC10 patch clamp amplifier (Dr. Schulze GmbH, Lambrecht, Germany) in the current clamp mode as described by others(3, 4). The liquid junction potential was calculated with the Clampex 10.0 software (Molecular Devices, Sunnyvale CA, USA) and an online correction was made for each recording. Both at baseline and during perfusion with 30 µM benzbromarone (BBR, Sigma, St Louis MO, USA) or 10 µM T16Ainh-A01 (Tocris, Bristol, UK), only those recordings in which (1) the E_m was constant for at least 3 minutes, and (2) the seal resistance was constantly high (> 5 GΩ) were used for the analyses.

Measurement of whole-cell Ca^{2+}-activated Cl^- current (I_{ClCa})

For the measurement of whole-cell I_{ClCa}, PASMC grown in T-25 tissue culture flasks were freshly harvested with StemPro Accutase (Life Technologies), centrifuged (300g, 5 min) and resuspended in Complete SMC Medium. PASMC were stored at 4°C until use and were allowed to attach to glass coverslips for 15-30 min at room temperature before the

measurements. Cells were perfused with a bath solution composed of (in mM) NaCl 150, glucose 10, HEPES 10, $CaCl_2$ 1, $MgCl_2$ 1, pH 7.4 (NaOH). The pipette solution contained (in mM) CsCl 110, TEA-Cl 20, EGTA 5, HEPES 10, Na_2ATP 1, $CaCl_2$ 4.68, $MgCl_2$ 1, pH 7.2 (NaOH). The free Ca^{2+} concentration of this solution was 2 µM as calculated with the MaxChelator software. In order to minimize K^+ current contamination of the recordings, after the formation of whole-cell configuration the bath solution was switched to a bath composed of (in mM) NaCl 140, glucose 10, HEPES 10, TEA-Cl 10, $CaCl_2$ 1, $MgCl_2$ 1, pH 7.4 (NaOH). In order to measure I_{ClCa}, the command potential was stepped from a 0 mV holding potential to -40, 0, +40, +80 and +120 mV for 1.5 s, allowing 0.5 s recovery time at the holding potential between each step. The average current measured between 750 and 1500 ms of each voltage step was plotted against the holding potential. Due to the almost symmetrical Cl^- concentration of the bath and pipette solutions, the reversal potential (E_{rev}) for Cl^- was expected to be around zero. Current recordings showing an E_{rev} significantly different from zero were considered as contaminated with K^+ currents and thus discarded. To study the effects of hypoxia, PASMC were incubated for 48 hr in a hypoxic incubator (1% O_2, 5% CO_2, 37°C), and harvested with StemPro Accutase as described previously, except that all solutions were pre-incubated in a hypoxic incubator for 1 hour, and harvesting was performed in a hypoxic workstation (1% O_2, 5% CO_2). The suspended PASMC were aliquotted into screw-cap glass tubes and kept at 4 °C until use. Before use, cells were allowed to attach to glass coverslips for 15-30 min in the hypoxic workstation at room temperature. Bath solutions were continuously bubbled with N_2. Cells from the same batch that were cultured, harvested and recorded under normoxic conditions served as controls.

For the experiments measuring the effect of benzbromarone on whole-cell I_{ClCa} after siRNA silencing, recordings were performed using an Axopatch-1D patch clamp amplifier (Axon Instruments, Inc., Foster City, CA, USA). Data were digitally sampled by a DigiData 1550B

(Axon Instruments, Inc.) A/D converter. Experiments were carried out at room temperature (21^{o}C). Solutions were applied using a gravity-driven perfusion system.

Assessment of PASMC proliferation *in vitro*

Human PASMC from Donor or IPAH lungs were seeded on 96-well plates. Cells were serum-starved for 12 hours, then underwent a 30 min pre-treatment with benzbromarone (30 µM), Temem16A activator (Eact; 1µM)or vehicle. After the pre-treatment, serum-free SMC Medium containing PDGF-BB (10 ng/ml, Sigma) and benzbromarone was applied. The proliferation was determined by [^{3}H]-thymidine incorporation (BIOTREND Chemikalien GmbH, Cologne, Germany) as an index of DNA synthesis, and detected with a scintillation counter (Wallac 1450 MicroBeta TriLux Liquid Scintillation Counter & Luminometer, PerkinElmer, Waltham MA, USA). Each independent experiment was performed in five replicates using PASMC isolated from six different donor and IPAH lungs.

In experiments using TMEM16A silencing, cells were first seeded on 6-well plates and transfected with TMEM16A siRNA or control non-silencing RNA as described above. Cells were re-seeded into 96-well plates 24 hours after transfection, starved for 12 hours, then the induction and measurement of proliferation was performed as detailed above.

Treatment of human PASMC with CLCA1-containing conditioned medium

The production and use of human CLCA1 protein containing conditioned medium was performed as described by a previous study (5), using HEK-293 cells to produce the conditioned medium. According to this study as well as our previous experience, HEK-293 can be transfected with high efficiency and have negligible endogenous CLCA1 expression. The identity of HEK-293 cells (#300192, CLS Cell Lines Service GmbH, Eppelheim, Germany) was verified by STR analysis and were negative for Mycoplasma. Cells were grown until 50% confluency in DMEM F-12 complete medium (ThermoFischer Scientific,

Vienna, Austria) containing 10% FCS (Lactan, Graz, Austria), 1% L-Glutamine and 0.2% antibiotics. The plasmide used for transfection was constructed by cloning the human CLCA1 gene into a pcDNA 3.1(+) vector. The HEK-293 cells were transfected overnight either with the CLCA1 gene containing or with the empty plasmid, using the Effectene transfection reagent kit (Qiagen) according to manufacturer's instructions, and DMEM F-12 complete medium. On the next day, the medium was changed to serum-free SMC Medium. The resulting conditioned media were collected 24 hours later and applied on the PASMC of healthy donors. After 24 hours of incubation, the E_m of the PASMC was measured as described above. To confirm the presence of CLCA1 in the conditioned medium, 20 µL of conditioned medium as well as control medium (collected from cells transfected with the empty plasmide) were analyzed with western blot as described above, using a CLCA1 antibody (ab108851, Abcam; shown in Supplementary Fig 3c). To verify equal sample loading, the membrane was stained with Coomassie Blue. A band at approx. 66 kDa appeared in both samples. We assumed this band corresponded to albumin and showed an equal density for both media as a verification for equal protein loading.

Measurement of pulmonary artery tone *ex vivo*

Pulmonary artery rings were isolated from male C57BL/6J mice (20–25 weeks old, Charles River, Wilmington MA, USA), as described by Jain et al(6). Following stable contraction (approx. 30 minutes post-addition of U-46619, 30 nM), the arteries were subjected to cumulatively increasing concentrations (0.1 to 30 µM) of the TMEM16A blockers T16Ainh-A01 (Tocris) and benzbromarone (Sigma) in order to analyze the concentration-response relationships.

Animal models of pulmonary hypertension (PH)

All animal studies conformed with the EU guidelines 2010/63/EU and were approved by the University Animal Care Committee and the federal authorities for animal research approved the study protocol (approval numbers: BMWFW-66.010/0144-WF/V/3b/2014, BMWFW-66.010/0076-WF/V/3b/2015). The ARRIVE guidelines were considered and all measures were taken to keep animal suffering to a minimum. Based on the 3R principle, mice of the control and HOX+Veh groups as well as rats from the control and MCT+Veh groups were utilized to assess the acute effects of benzbromarone (described later and illustrated on Figures 4a and 5a), in order to reduce the total number of animals needed. The minimum numbers of animals in each group were determined using power calculations and data from previous experiments.

Chronic hypoxia-induced mouse model of PH

The experimental protocol is depicted in Figure 4a. Male C57BL/6J mice (Charles River) at the age of 10 weeks were either placed into a hypoxic chamber (FiO_2=0.1, n=16) for 4 weeks, or kept at normoxic conditions (control group, FiO_2=0.21, n=8). According to the reports of Fagan *et al.* (7) and Tuscherer *et al.*(8), a significant increase in the right ventricular systolic pressure (RVSP) and PA muscularization can be observed already after 14 days of hypoxia exposure. Therefore, mice subjected to hypoxia were randomized into two groups at the end of the second week. Eight mice received a subcutaneous slow-release pellet containing benzbromarone (Innovative Research of America, Sarasota FL, USA) (HOX+BBR) and the other 8 mice received pellets with vehicle (HOX+Veh). The pellets ensured a stable blood concentration of the drug/vehicle over the next two weeks. At the end of week 4, all mice were subjected to *in vivo* hemodynamic measurements, followed by sacrifice and organ collection.

Monocrotaline treated rats

The experimental protocol is shown in Figure 5a. Male Sprague-Dawley rats (body weight: approx. 250 g, Charles River) received a single subcutaneous injection of monocrotaline (MCT, 60 mg/kg, n=16) or vehicle (control group, n=8). Since significant RVSP increase and PA muscularization had been detected as early as 12 days after the injection of MCT(9), two weeks after monocrotaline treatment rats were randomly ordered into two groups. Subcutaneous slow-release pellets (Innovative Research of America) that contained either benzbromarone (MCT+BBR, n=8) or vehicle (MCT+Veh, n=8) were implanted. Four weeks after monocrotaline treatment all rats were subjected to echocardiography and *in vivo* hemodynamic measurements, thereafter they were sacrificed for organ collection.

Echocardiography

Echocardiographic measurements were performed using a Vevo 770 High Resolution Imaging System with a 30 MHz RMV-707B scan head (VisualSonics, Toronto, Canada) as previously reported (10). Briefly, animals were mounted on a heated pad and kept under anaesthesia with isoflurane 0.8-1.2%. Chest hair was depilated and a layer of sonographic coupling gel was applied to the thorax. RV internal diameter (RVID) and free wall thickness (RVFW) from the left parasternal long axis view were measured in M-mode and 2-D modalities. RV outflow tract was visualized from the parasternal short axis view at the level of the aortic valve. From this view, pulse wave (PW) Doppler flow recordings of the pulmonary artery were obtained with the sample volume positioned at the tip of the pulmonary valve leaflets. Here, peak velocity, acceleration time (PAAT), and velocity-time integral (VTI) were measured. For every parameter, measurements were done for 4-5 cardiac cycles and results were averaged. Cardiac output was calculated as CO (mL/min) = (7.85 × [RV outflow tract]2 × pulmonary valve velocity-time integral × heart rate)/1,000. Cardiac

index (CI) was obtained by normalizing cardiac output to body weight. The operator was blinded to the experimental group: animals were identified with number codes that did not carry information about the treatment they previously undergone.

In vivo hemodynamics

Mice

In vivo hemodynamics was performed under constant inhalation of 2% isoflurane/oxygen, using the closed chest technique through a small incision on the submandibular area. Body temperature was monitored and maintained at 37 ± 1 °C. A limb-lead ECG was recorded and the heart rate was kept constant to avoid changes in the sympathetic tone during the experiment. The right ventricle (RV) was catheterized via the right jugular vein using a 1.4 F Millar catheter (SPR-671, Millar, Houston TX, USA) and right ventricular systolic pressure (RVSP) was measured continuously. Another catheter was inserted into the left carotid artery to monitor systemic blood pressure. After recording of stable values, the experiment was either continued with the assessment of the acute hemodynamic effects of benzbromarone (described above), or mice were sacrificed immediately for organ collection. Animals were identified with a number code throughout the experiment to ensure that the operator was blinded for the experimental groups.

Acute hemodynamic effects of benzbromarone in mice

Mice of the above-described control and HOX+Veh groups were used for these studies. Benzbromarone was injected into the left jugular vein as a single bolus (300 µm, i.v. in 50 µl saline) and pressures were monitored until a maximum effect was observed (approx. 10 minutes post-injection). Only those mice that maintained a stable RVSP both before and 10 min after the BBR application were included in the analysis.

Rats

In vivo hemodynamic measurements were conducted as described above for the mice, with the exception that for the right ventricular and the systolic blood pressures, 2 F Millar Catheters (SPR-513 and SPR-320, respectively) were used.

Acute hemodynamic effects of benzbromarone in rats

The above described control and MCT+Veh groups were included in this study. Benzbromarone was injected into the left jugular vein as a single bolus (300 µm, i.v. in 100 µl saline) and pressures were monitored until a maximum effect was observed (approx. 10 minutes). Rats that failed to maintain a steady-state RVSP either before or after BBR injection were excluded from this analysis.

Assessment of right ventricular hypertrophy

At the end of the hemodynamic measurements, animals were exsanguinated and the heart and lungs were isolated. The right ventricle (RV) was dissected from the left ventricle + septum (LV+S) and both of them were weighed. Right ventricular hypertrophy was assessed by calculating the Fulton index, defined as RV weight/(LV+S weight).

Immunohistological assessment of vascular remodeling and cell proliferation

Paraffin-embedded mouse and rat lung tissues were cut to 2 µm thin sections. Double immunohistochemical staining and quantification of the non-muscularized and muscularised arteries were made as previously described (11). Immunostained slides were scanned with an Olympus BX61VS microscope using the OlyVIA software (Olympus Austria GmbH, Vienna, Austria). Vessel remodeling in lung sections was quantified using semi-automated image analysis software (Visiopharm, Hoersholm, Denmark). Throughout the analysis, all samples were identified with number codes to make sure the oparator was blinded for the experimental

group. The percentage of non-muscularized and muscularised pulmonary arteries, relative to the total number of pulmonary arteries, was calculated.

Serial sections from the same lungs were used to determine cell proliferation in the PA wall, as described by Zabini *et al*(12). Lung sections were labeled using a primary antibody against the proliferation marker PCNA (sc-7907, Santa Cruz). Immunostained slides were scanned with an Olympus BX61VS microscope equipped with the OlyVIA software (Olympus Austria GmbH, Vienna, Austria). Negative controls were performed with the omission of the primary antibody.

Assessment of the hemodynamic effect of a single oral dose of benzbromarone in IPAH patients

The study protocol (Clinical trial registration number: NCT02790450; EudraCT number: 2015-000709-38) was approved by the Ethics Committee of the Medical University of Graz. According to the convention for human pharmacological pilot studies, 10 IPAH patients were involved; for ethical reasons, we did not establish a placebo group in this study. All patients provided a written informed consent to participate in the study. Examinations were performed by the same experienced team. For the right heart catheterizations, a 7F quadriple-lumen, balloon-tipped, flow-directed Swan-Ganz catheter (Baxter, Deerfield, IL) was introduced using the transjugular approach. Hemodynamic measurements included systolic, diastolic and mean pulmonary arterial pressure, pulmonary arterial wedge pressure, right atrial pressure, and cardiac output measured by the thermodilution technique and calculated using an analog computer system. Pulmonary vascular resistance was derived from the difference of mean pulmonary arterial pressure and pulmonary arterial wedge pressure divided by cardiac output. Cardiac index was determined as the ratio of cardiac output to body surface area. All measurements were performed in the supine position, pressure values were continuously recorded and averaged over several respiratory cycles during spontaneous breathing. Zero

reference level was set at mid-thoracic level). Partial pressure of oxygen and oxygen saturation of arterialized ear lobe capillary blood and pulmonary arterial blood were determined with an ABL 800 Flex (Radiometer; Copenhagen, Denmark) blood gas analyzer. Systemic blood pressure was measured by a sphygmomanometer.

Assessment of CLCA1 concentration in human plasma and lung homogenate

Plasma samples from 10 IPAH patients at the time of right heart catheterization, as well as from 10 age- and sex matched healthy controls were collected. A written informed consect was obtained from each patient prior to the interventions. The study was carried out under the clinical trial registration number NCT01607502, and was approved by the Ethics Committee of the Medical University of Graz. For patient's characteristics see Table E3. Samples were diluted 1:5 with PBS and the concentration of CLCA1 was determined using the Human CLCA1 ELISA Kit (Abbexa, Cambridge, UK). In order to determine the CLCA1 concentration in lung homogenates, frozen lung tissue pieces from 8 IPAH patients and 8 healthy donors (Characteristics of these patients are given in Table E1) were homogenized on liquid nitrogen and dissolved in PBS. A freeze-thaw cycle and sonication were applied to disrupt the cell membranes, followed by a centrifugation at 8000 g for 5 min. The supernatans, without dilution, were analyzed as described above.

Statistical analyses

Data are shown either as individual data plots with median, or summarized as mean ± s.e.m. In the case of summarized data, n numbers for each group are given in the corresponding figure legend. Statistical analyzes were performed using Prism 6.0 (GraphPad Software, La Jolla, CA), statistical tests were selected to be appropriate for the given dataset, and are identified in the corresponding figure legend. All datasets met the assumptions of the

statistical test used and compared groups had similar variance. For all datasets, statistical analyses were two-sided, and P values <0.05 were considered significant.

Supplementary Tables

Lung ID	Age (years)	Sex (M/F)	mPAP (Hgmm)	Material used
Donor 1	44	F		LCM-PA
Donor 2	43	F		LCM-PA, LT
Donor 3	40	F		LCM-PA, LT
Donor 4	16	M		LCM-PA, PASMC, LT
Donor 5	18	M		LCM-PA, PASMC
Donor 6	62	M		LCM-PA, LT
Donor 7	59	M		LCM-PA, PASMC
Donor 8	49	M		LCM-PA, PASMC
Donor 9	47	M		PASMC
Donor 10	50	F		PASMC
Donor 11	48	M		PASMC
Donor 12	22	M		PASMC
Donor 13	42	F		PASMC, LT
Donor 14	9	M		PASMC
Donor 15	31	M		PASMC
Donor 16	30	M		PASMC
Donor 17	60	F		PASMC
Donor 18	70	F		LCM-PA, LT
Donor 19	58	F		LCM-PA, LT
Donor 20	3	M		LCM-PA
Donor 21	24	F		LCM-PA
Donor 22	52	M		LCM-PA
Donor 23	19	M		LCM-PA
Donor 24	71	F		LCM-PA
Donor 25	53	F		LCM-PA, LT
Donor 26	56	F		LCM-PA
Donor 27	49	M		PASMC

Donor 28	57	M		PASMC
Donor 29	46	F		PASMC
Donor 30	46	M		PASMC
IPAH 1	31	F	50	LCM-PA, PASMC, LT
IPAH 2	14	F	154*	LCM-PA
IPAH 3	37	F	88	LCM-PA, PASMC, LT
IPAH 4	20	F	56	LCM-PA, PASMC
IPAH 5	25	F	87	LCM-PA, PASMC, LT
IPAH 6	39	F	54	LCM-PA, LT
IPAH 7	32	F	77	LCM-PA, PASMC, LT
IPAH 8	36	M	64	PASMC, LT
IPAH 9	9	F	98	PASMC
IPAH 10	50	M	70	LCM-PA, PASMC
IPAH 11	13	M	91	PASMC
IPAH 12	38	F	102	PASMC, LT
IPAH 13	27	F	70	LCM-PA, PASMC
IPAH 14	34	F	95	LCM-PA
IPAH 15	52	F	65	LCM-PA, LT
IPAH 16	34	F	69	LCM-PA
IPAH 17	41	M	101	LCM-PA
IPAH 18	21	M	74	LCM-PA

Table E1. Age, sex and mean pulmonary arterial pressure (mPAP, when known) of healthy lung transplant donors and recipient IPAH patients. The materials used from each lung (LCM-PA: laser capture microdissected pulmonary artery; PASMC: pulmonary arterial smooth muscle cell, LT: lung tissue) are shown. *: Right heart catheterization data was not available for this patient, the sPAP was estimated from echocardiography performed before lung transplant.

Gene	Acc. Number	Forward primer	Reverse primer	Product size (bp)
ANO1	XM_011545121.1	CACGATGAGGGTCAACGAGA	ATAAGGAGTTCAGCAGCGTG	128
LRRC8A	NM_001127244.1	GGGTTGAACCATGATTCCGGTGAC	GAAGACGGCAATCATCAGCATGAC	133
LRRC8B	NM_001134476.1	ACCTGGATGGCCCACAGGTAATAG	ATGCTGGTCAACTGGAACCTCTGC	126
LRRC8C	NM_032270.4	ACAAGCCATGAGCAGCGAC	GGAATCATGTTTCTCCGGGC	132
LRRC8D	NM_001134479.1	ATGGAGGAGTGAAGTCTCCTGTCG	CTTCCGCAAGGGTAAACATTCCTG	126
LRRC8E	NM_025061.5	ACCGTGGCCATGCTCATGATTG	ATCTTGTCCTGTGTCACCTGGAG	62
NKKC1	NM_001046.2	TGAACCTCTTCGTGGCTACAT	GCAAGTGATGCATGGAATACTGA	150
KCC1	NM_005072.4	GCTCAGTTGGGTGGACTACG	CAGCTCTTCCTCAAACAGTGC	154
KCC3	NM_001042496.1	AAGCCGGAGTGAGCCTATGA	GCTGTGTTCCCCTGTGATGG	145
KCC4	NM_006598.2	ATGAAGCCGGACCAGTCCAA	GGAGGACCTGGCATGTTGAG	116
AE2	NM_003040	ACCCAGGAGATCTTCGCCTT	GTCCACCTCTGAGCTGTTGG	126
CFTR	NM_000492.3	TTAATGCCCTTCGGCGATGT	AGCGTTCCTCCTTGTTATCCG	144
CLCN3	NM_001243374.1	GGATGCTTCTTCCGACCCT	GAACTGTTAATGCTGCCTCCA	120
CLIC-2	NM_001289.4	CAGGTACCAATCCTCCGTTCC	TCAGGTGAGGGTACCTTGGA	111
CLIC-3	NM_004669.2	TGCACATCGTCGACACGG	TGTGCGGACACGTGTATTTG	126

CLIC-4	NM_013943.2	CTGAATGGGCTGAAGGAGGA	ATGAAGAGCCTCTGGGAAAAGG	110
Exon 6b-detect	XM_011545121.1	AACGACGTGTACAAAGGCCA	ATCGTGCAGTGGGTATGCAG	154
Exon 6b-missing	XM_011545121.1	GTACAGCATGGGCATCACGA	AGGTCGATGGGCTGGTACTT	168
Exon 13-detect	XM_011545121.1	TCTGTCTTCATGGCCCTCTG	ATGATCCTTGACAGCCTCCTC	123
Exon 13-missing	XM_011545121.1	CAGCCACCTCTTCGACAACC	GGATGATCCTCTTCCTCTTCAAAGC	150
Exon 15-detect	XM_011545121.1	AGAGCTGAATACGAAGCCAGA	GCCATGGCTGTCTTAACCCT	128
Exon 15-missing	XM_011545121.1	TCCTAGAGCTGAATACGAAGCC	TGTCAGTCTCTTTGTTTCTGGACT	74
B2-M	NM_004048	TGGAGGCTATCCAGCGTACT	TGTCGGATGGATGAAACCCA	111

Table E2. Primers used to assess the expression of Cl- channel and transporter genes or the alternative splicing of the ANO1 gene (Exon "detect" and "missing" primers). Gene name, PubMed Nucleotide accession number used for primer design, forward and reverse primer sequences and the size of the PCR product (in bp) are given. All primers were designed so that the PCR product span at least one exon-exon junction.

Sample ID	Age (years)	Sex (M/F)	mPAP (Hgmm)
Control 1	71	F	
Control 2	72	F	
Control 3	58	F	
Control 4	77	F	
Control 5	35	F	
Control 6	44	F	
Control 7	70	M	
Control 8	75	F	
Control 9	43	F	
Control 10	89	F	
IPAH 1	37	F	24*
IPAH 2	45	F	51
IPAH 3	48	F	43
IPAH 4	72	F	47
IPAH 5	56	F	39
IPAH 6	73	F	45
IPAH 7	70	M	49
IPAH 8	84	F	42
IPAH 9	79	F	45
IPAH 10	69	F	41

Table E3. Age, sex and mean pulmonary arterial pressure (mPAP, when known) of those control and IPAH patients whose plasma was used for the CLCA1 ELISA measurement. *IPAH1 is an IPAH patient fulfilling responder criteria and is under high-dose calcium antagonist therapy. At the time of hemodynamic substudy Ca^{2+} channel antagonist therapy was stopped, however her mPAP values still remained below 25mmHg.

Patient ID	Age (years)	Sex	mPAP (Hgmm)	NYHA Class
Patient #1	50	Female	49	2
Patient #2	37	Female	23*	2
Patient #3	59	Female	31	2
Patient #4	74	Female	51	2
Patient #5	69	Female	35	3
Patient #6	76	Female	31	2
Patient #7	73	Male	66	3
Patient #8	57	female	46	2

Table E4. Age, sex, mPAP and NYHA Class of the IPAH patients subjected to right heart catheterization to measure the hemodynamic effects of a single acute dose of benzbromarone (BBR). *Patient #2 is an IPAH patient fulfilling responder criteria and is under high-dose calcium antagonist therapy. At the time of hemodynamic substudy Ca^{2+} channel antagonist therapy was stopped, however her mPAP values still remained below 25mmHg.

Parameter	Baseline		120 min BBR		p value
	mean	95% CI	mean	95% CI	
HR (bpm)	67.7	58.8 – 76.7	68	60.2 – 75.8	0.833
mPAP (Hgmm)	41.5	29.8 – 53.2	45.7	32.7 – 58.8	0.007*
sSBP (Hgmm)	115.6	105.8 – 125.4	118	104.1 – 131.9	0.461
dSBP (Hgmm)	62.1	52.7 – 71.5	65.5	54.8 – 76.2	0.172
PAWP (Hgmm)	7.3	4.95 – 9.7	7.4	4.55 – 10.2	0.785
CO (l/min)	4.3	3.4 – 5.1	4.2	3.5 – 4.9	0.692
RAP (Hgmm)	4.9	2.0 – 7.8	4.98	2.0 – 7.7	1.000
PVR (Wood unit)	8.9	4.2 – 13.7	9.9	5.2 – 14.5	0.031*
SpO_2 (%)	92.6	89.6 – 95.5	92.3	88.9 – 95.7	0.444

Table E5. Hemodynamic parameters before and 120 min after a single-dose, acute administration of benzbromarone (BBR; 200 mg per os). Abbreviations: HR – heart rate, mPAP – mean pulmonary arterial pressure, sSBP – systolic systemic blood pressure, dSBP – diastolic systemic blood pressure, PAWP – pulmonary arterial wedge pressure, CO – cardiac output, RAP – right atrial pressure, PVR – pulmonary vascular resistance, SpO2 – peripheral oxygen saturation. *: $p < 0.05$, paired t test.

Parameter	Control	MCT+Veh	MCT+BBR	p (Control vs MCT+Veh)	p (MCT+Veh vs MCT+BBR)
RVFW Thickness (mm)	0.30 ± 0.02	0.42 ± 0.03	0.30 ± 0.02	<0.05	<0.05
RVID (mm)	2.77 ± 0.2	3.92 ± 0.3	3.10 ± 0.1	<0.01	>0.05
CI (ml/min/100g)	0.34 ± 0.01	0.27 ± 0.02	0.35 ± 0.01	<0.05	<0.01
CO (ml/min)	143.5 ± 7.8	105.3 ± 9.0	128.8 ± 5.5	<0.01	>0.05
PAAT (ms)	29.3 ± 1.1	20.6 ± 1.9	28.2 ± 1.4	<0.01	<0.01
BW (g)	448.4 ± 5.4	385.8 ± 11.8	368.9 ± 4.5	<0.001	<0.001

Table E6. Echocardiography parameters measured in the experiment described on Figure 6. RVFW Thickness: right ventricular free wall thickness; RVID: right ventricle inner diameter; CI: cardiac index; CO: cardiac output; PAAT: pulmonary arterial acceleration time; BW: body weight. Data are given as mean ± SEM. P values were calculated using one-way ANOVA and Bonferroni's Multiple Comparison Test.

Supplementary References

(1) Hoffmann J, Wilhelm J, Marsh LM, Ghanim B, Klepetko W, Kovacs G, Olschewski H, Olschewski A, Kwapiszewska G. Distinct differences in gene expression patterns in pulmonary arteries of patients with chronic obstructive pulmonary disease and idiopathic pulmonary fibrosis with pulmonary hypertension. *Am J Respir Crit Care Med* 2014;190:98-111.

(2) Stulnig G, Frisch MT, Crnkovic S, Stiegler P, Sereinigg M, Stacher E, Olschewski H, Olschewski A, Frank S. Docosahexaenoic acid (DHA)-induced heme oxygenase-1 attenuates cytotoxic effects of DHA in vascular smooth muscle cells. *Atherosclerosis* 2013;230:406-413.

(3) Mason MJ, Simpson AK, Mahaut-Smith MP, Robinson HP. The interpretation of current-clamp recordings in the cell-attached patch-clamp configuration. *Biophys J* 2005;88:739-750.

(4) Perkins KL. Cell-attached voltage-clamp and current-clamp recording and stimulation techniques in brain slices. *J Neurosci Methods* 2006;154:1-18.

(5) Sala-Rabanal M, Yurtsever Z, Nichols CG, Brett TJ. Secreted CLCA1 modulates TMEM16A to activate Ca(2+)-dependent chloride currents in human cells. *Elife* 2015;4:10.7554/eLife.05875.

(6) Jain PP, Leber R, Nagaraj C, Leitinger G, Lehofer B, Olschewski H, Olschewski A, Prassl R, Marsh LM. Liposomal nanoparticles encapsulating iloprost exhibit enhanced vasodilation in pulmonary arteries. *Int J Nanomedicine* 2014;9:3249-3261.

(7) Fagan KA, Oka M, Bauer NR, Gebb SA, Ivy DD, Morris KG, McMurtry IF. Attenuation of acute hypoxic pulmonary vasoconstriction and hypoxic pulmonary hypertension in mice by inhibition of Rho-kinase. *Am J Physiol Lung Cell Mol Physiol* 2004;287:L656-64.

(8) Tuchscherer HA, Vanderpool RR, Chesler NC. Pulmonary vascular remodeling in isolated mouse lungs: effects on pulsatile pressure-flow relationships. *J Biomech* 2007;40:993-1001.

(9) Rosenberg HC, Rabinovitch M. Endothelial injury and vascular reactivity in monocrotaline pulmonary hypertension. *Am J Physiol* 1988;255:H1484-91.

(10) Egemnazarov B, Schmidt A, Crnkovic S, Sydykov A, Nagy BM, Kovacs G, Weissmann N, Olschewski H, Olschewski A, Kwapiszewska G, Marsh LM. Pressure Overload Creates Right Ventricular Diastolic Dysfunction in a Mouse Model: Assessment by Echocardiography. *J Am Soc Echocardiogr* 2015;28:828-843.

(11) Crnkovic S, Hrzenjak A, Marsh LM, Olschewski A, Kwapiszewska G. Origin of neomuscularized vessels in mice exposed to chronic hypoxia. *Respir Physiol Neurobiol* 2011;179:342-345.

(12) Zabini D, Crnkovic S, Xu H, Tscherner M, Ghanim B, Klepetko W, Olschewski A, Kwapiszewska G, Marsh LM. High-mobility group box-1 induces vascular remodelling processes via c-Jun activation. *J Cell Mol Med* 2015;19:1151-1161.

Figure Legends for Online Supplementary Figures

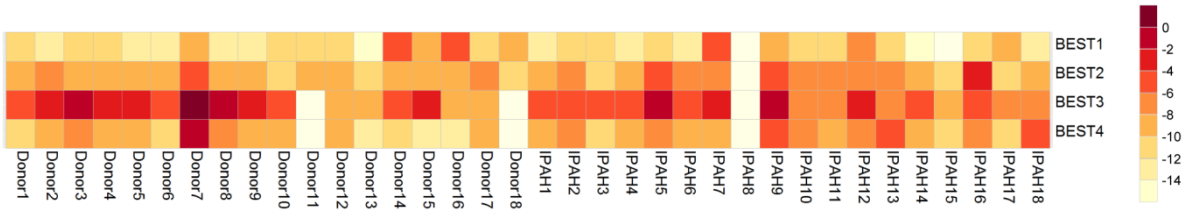

Figure E1 Bestrophin RNA expression in Laser cut material from Donor (n=18) and IPAH (n=18) pulmonary arteries

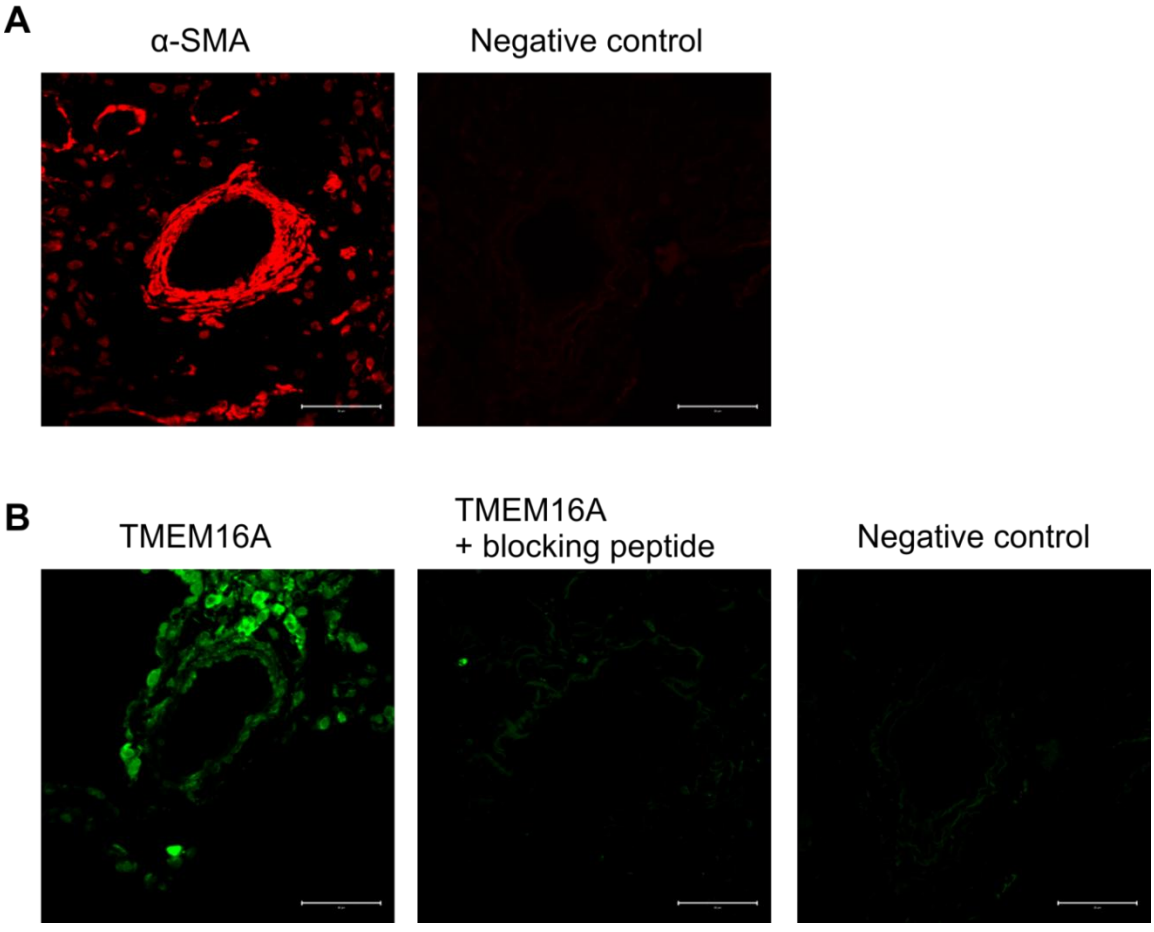

Figure E2. Negative controls of the immunofluorescence stainings shown on Figure 1d.

(A) Lung tissue from a donor labeled for α-smooth muscle actin (left) and the same labeling without primary antibody as negative control. **(B)** Donor lung tissue labeled for TMEM16A (left), labeling with TMEM16A primary antibody that was pre-incubated with the control antigen peptide (blocking peptide, middle), and labeling when primary antibody was omitted as a negative control (right). Scale bar, 50 µm.

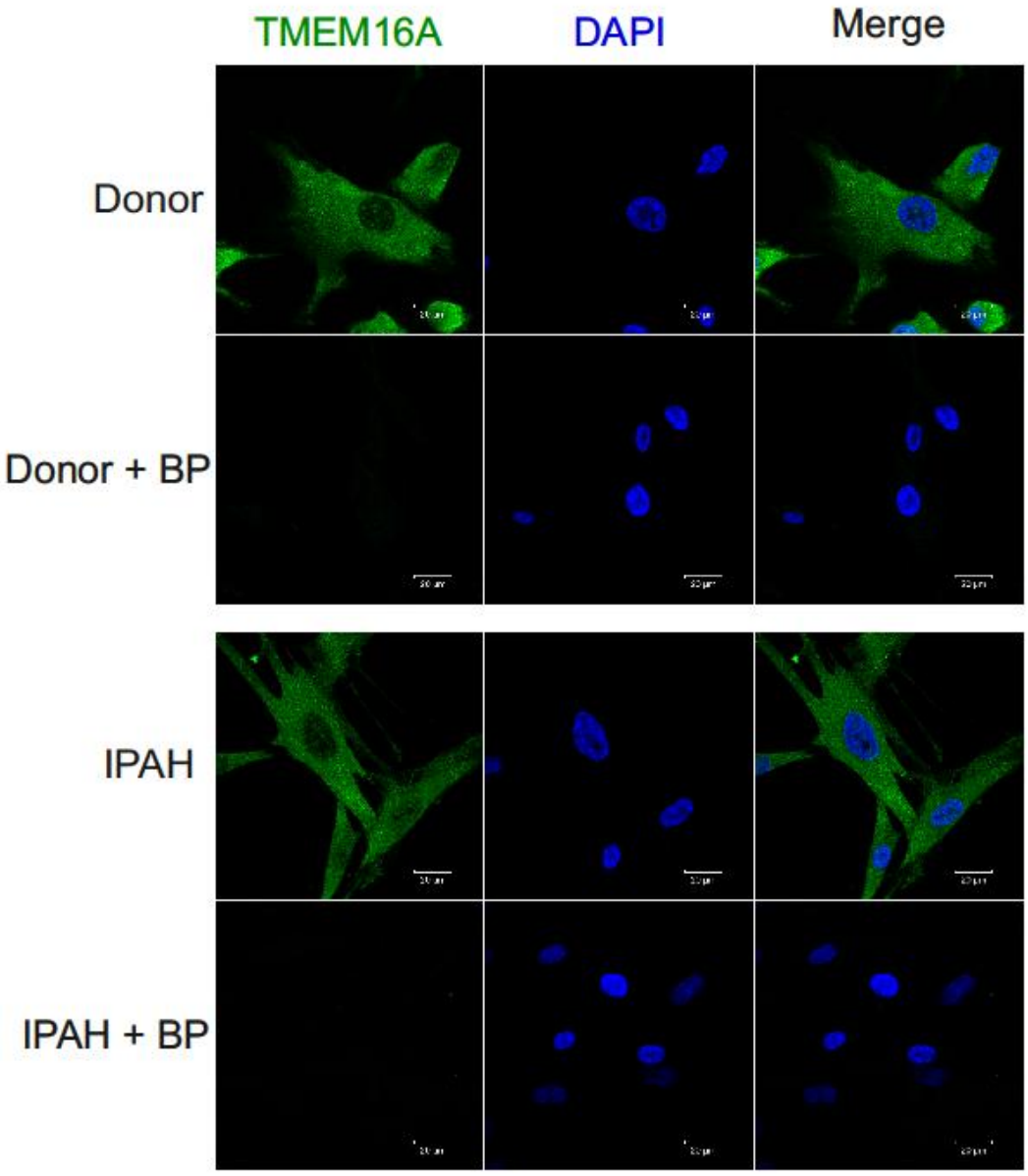

Figure E3. Presence of TMEM16A protein in the primary PASMC of donors and IPAH patients.

Primary PASMC from donors and IPAH patients labeled for TMEM16A. The nuclei were counterstained with DAPI. As a control a blocking peptide (BP) was added to the primary antibody. Scale bar, 20 µm.

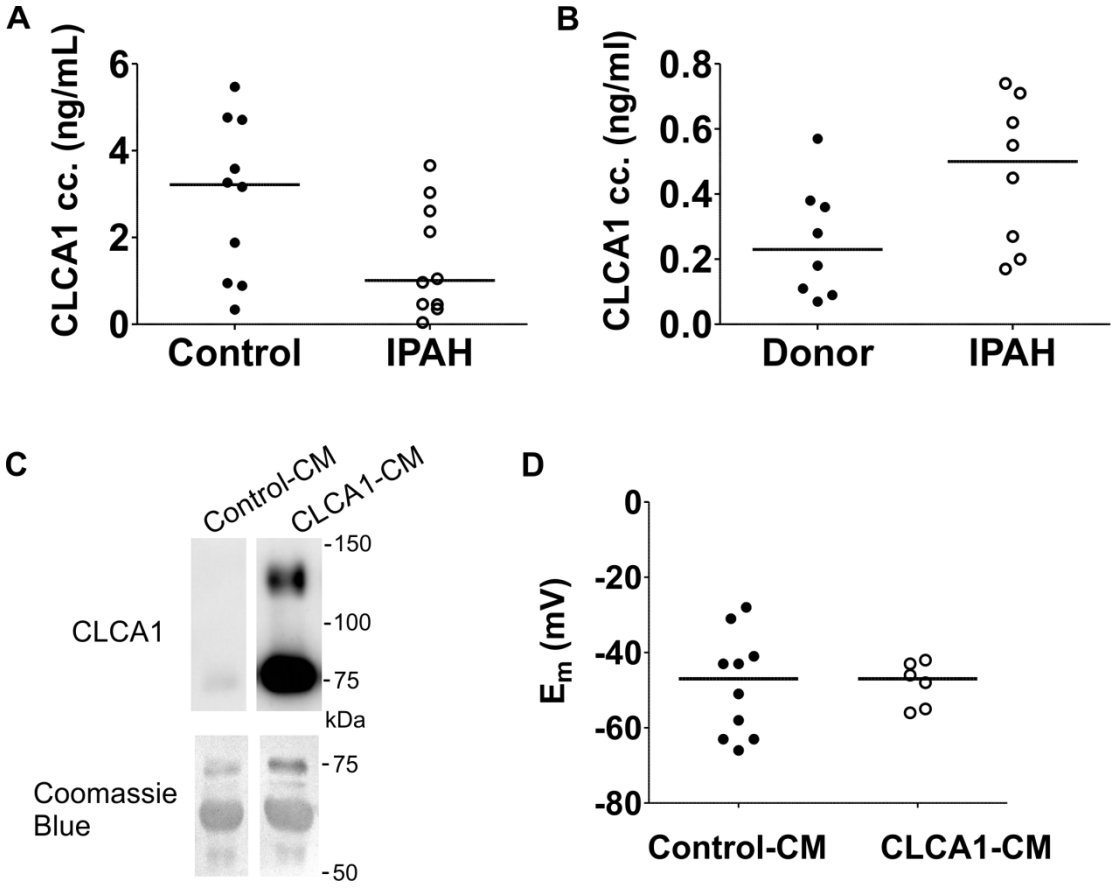

Figure E4. Assessment of the CLCA1-TMEM16A signaling in donors and IPAH patients.

(A) Concentration of CLCA1 in the plasma of IPAH patients compared to healthy controls. **(B)** CLCA1 concentration measured in IPAH as well as in healthy donor lungs. **(C)** Presence of CLCA1 in the conditioned medium, verified with Western blot. Conditioned medium (CM) was collected from HEK-293 cells transfected either with an empty vector (Control-CM) or a vector containing the CLCA1 gene (CLCA1-CM). Coomassie Blue staining of the membrane was used as loading control. **(D)** Resting membrane potential (E_m) of donor PASMC treated either with control (Control-CM) or CLCA1-containing conditioned medium (CLCA1-CM) for 24 hours.

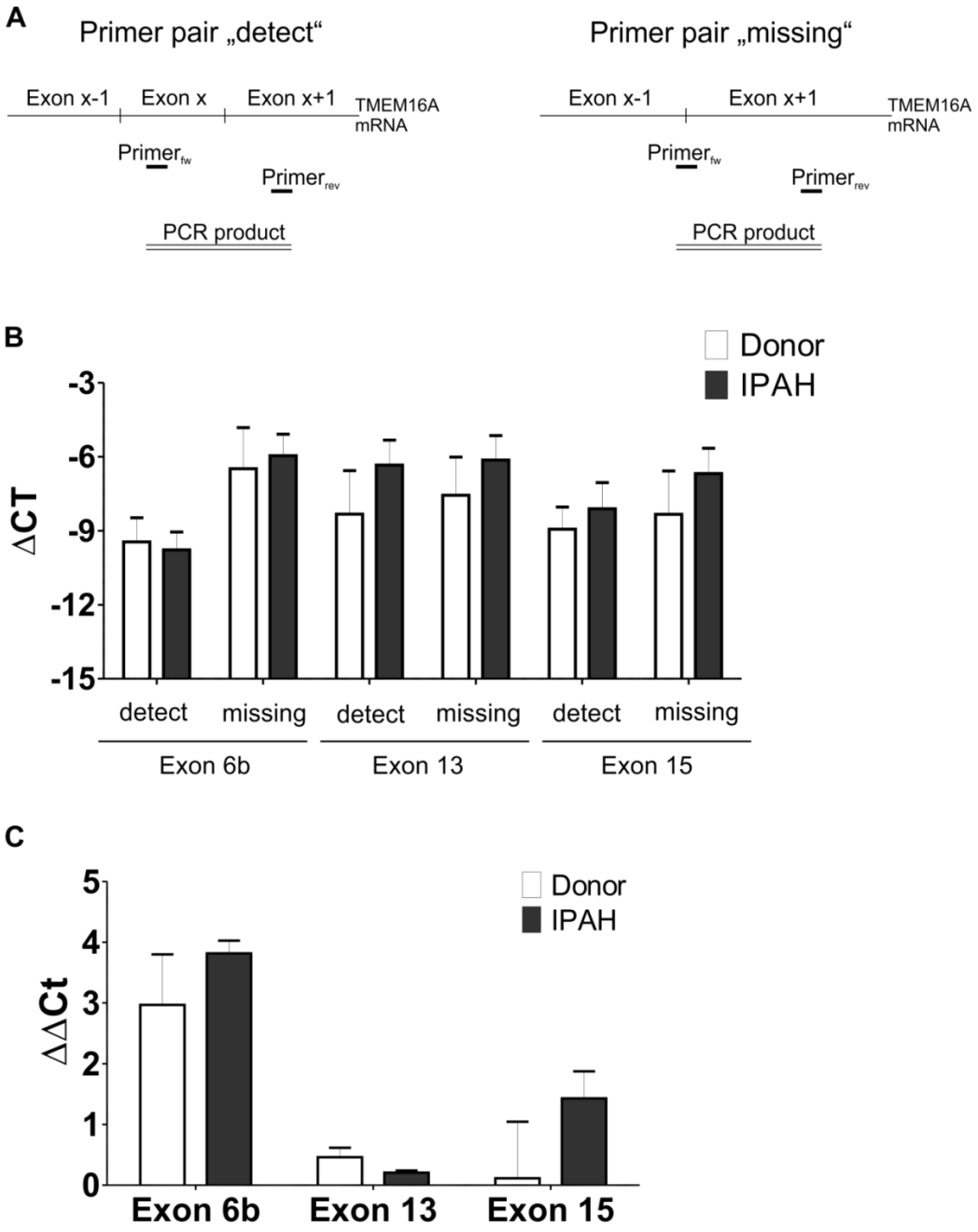

Figure E5. Expression of different *ANO1* splice variants.

(A) Schematics of primer design for studies of alternative splicing. Primer pairs “detect” were designed to detect the presence of the studied exon. In contrast, primer pairs “missing” resulted in

a PCR product only in the absence of the studied exon. **(B)** Expression of alternatively spliced exons of the TMEM16A gene. All three exons were analyzed with primer pairs specific for the presence (detect) or the absence (missing) of the exon. ΔCt values have been calculated as the difference of TMEM16A and β2 microglobulin expression (Donor n=5, IPAH n=6). **C:** ΔΔCt values calculated as $\Delta Ct_{missing}$-ΔCt_{detect}.

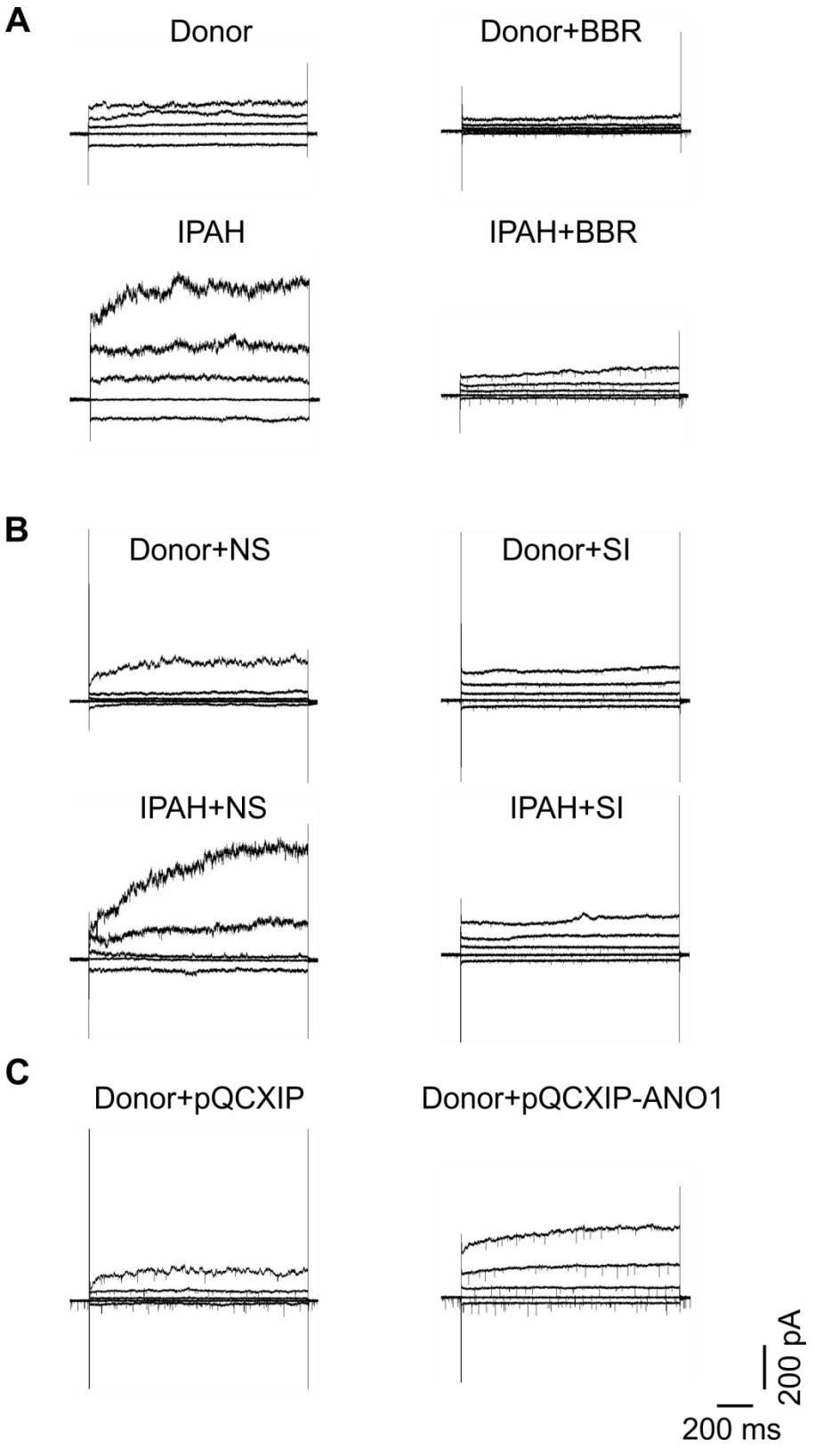

Figure E6. Representative I_{ClCa} recordings.

(A) Representative I_{ClCa} traces recorded in the PASMC of donors and IPAH patients with and without perfusion with 30 µM benzbromarone (BBR), and **(B)** 72 hours after transfection with non-silencing control RNA (NS) or siRNA against TMEM16A (SI). **(C)** Representative I_{ClCa} traces recorded in the PASMC of donors 72 hours after transfection with either empty or TMEM16A gene (*ANO1*) containing pQCXIP plasmide (pQCXIP or pQCXIP-ANO1, respectively).

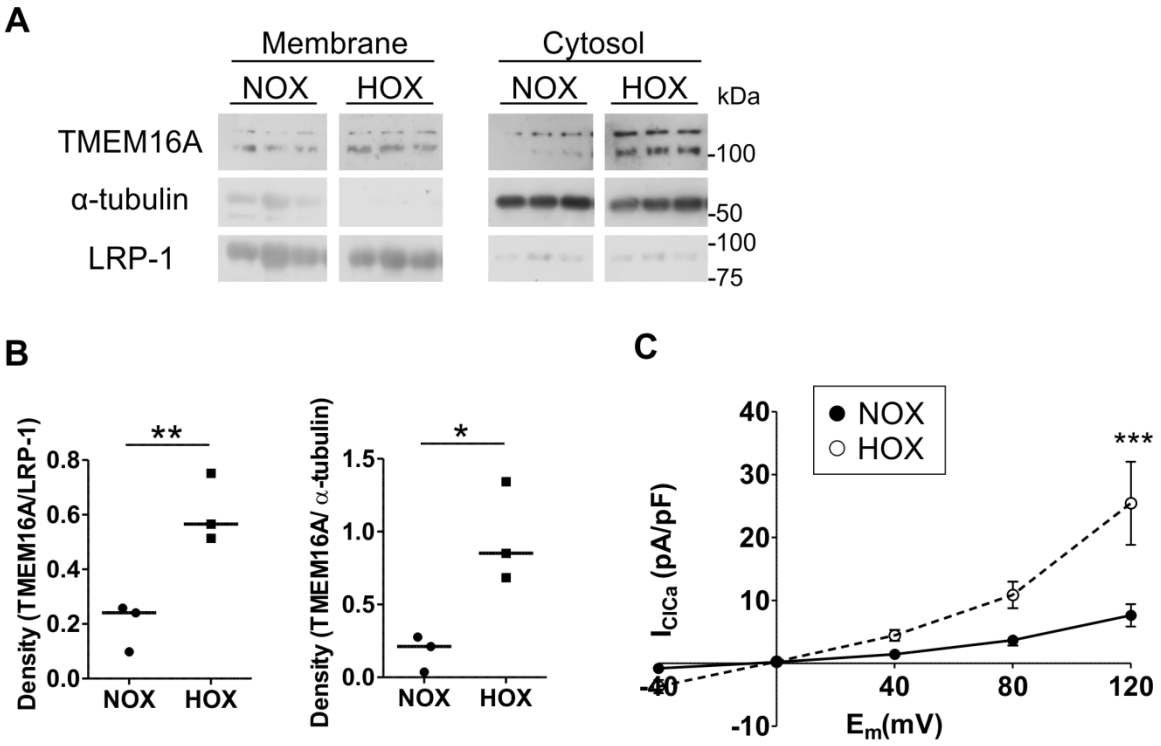

Figure E7. Effect of hypoxia on sarcolemmal TMEM16A protein levels and I_{ClCa} density.

(A) TMEM16A protein expression in the membrane and the cytosolic fractions analyzed with western blot**. (B)** Densitometric quantification. **(C)** Whole-cell I_{ClCa} in donor PASMC after 48 hrs of hypoxia, compared to cells cultured under normoxic conditions (n=6 for normoxia and n=8 for hypoxia). * $p < 0.05$, ** $p < 0.01$, *** $p < 0.001$, unpaired t test in **B**, two-way-ANOVA with Bonferroni post test in **C**.

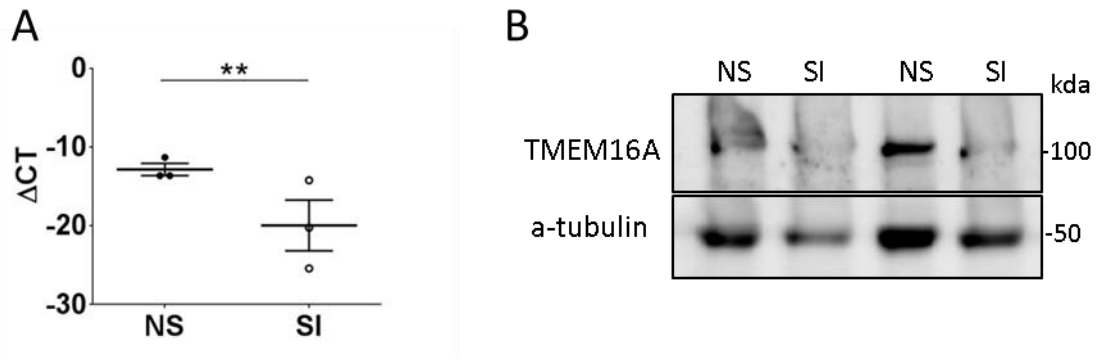

Figure E8. Silencing of TMEM16A in IPAH PASMCs.

(A, B) TMEM16A mRNA expression **(A)** and total protein level **(B)** in PASMC treated with either non-silencing control RNA (NS) or TMEM16A siRNA (SI). mRNA expression was studied 48 hours post-transfection and is given as ΔCt, calculated as the difference of TMEM16A and β2 microglobulin expression. (n IPAH = 3-4, unpaired t test ** $p < 0.01$)

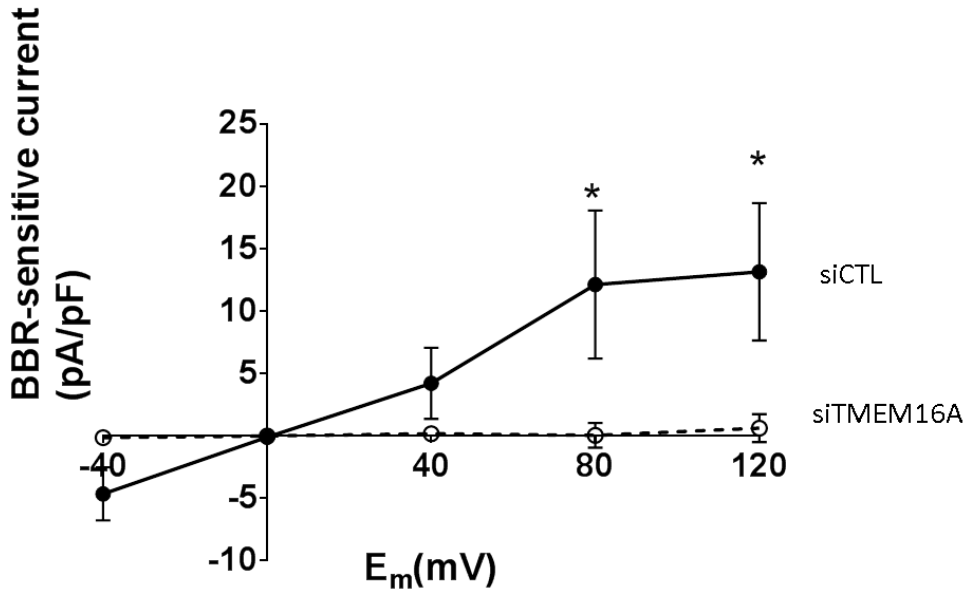

Figure E9. Effect of TMEM16A silencing on the BBR-sensitive current

Averaged I-V curves (mean±S.E.M) of the BBR-sensitive current (30µM BBR) in IPAH PASMC (n=5 cells from 2 patients) transfected with either control (siCTL) or TMEM16A siRNA (siTMEM16A). two-way ANOVA with Bonferroni post-hoc test was performed (* $p < 0.05$).

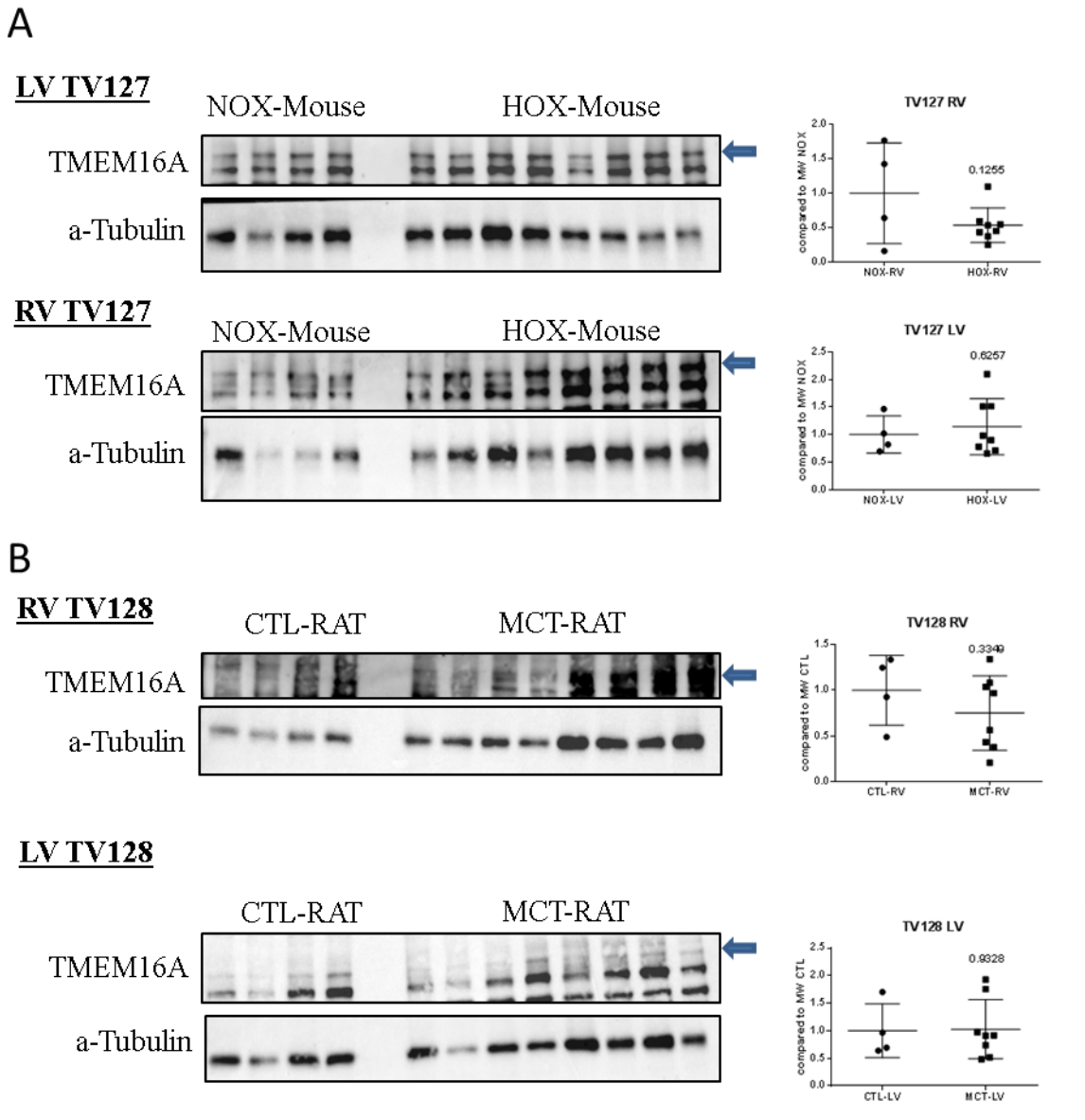

Figure E10: Western blots showing TMEM16A and alpha-tubulin protein expression in the left (LV) and right (RV) heart ventricle taken from normoxic (n=4) versus hypoxic (n=8) treated mice (A) and control vs monocrotaline treated rats (B). Quantification of each blot is shown next to the western blots.